

Responses to reviewers' comments

We would like to thank the reviewers for their valuable and constructive feedbacks and comments, which helped us to improve the manuscript.

Referee comments are given in black, and our responses are in blue. Changes made to the manuscript are marked in underlined blue. The line number referred here is for the new revised manuscript.

Anonymous Referee #1

This manuscript reports a novel “binPMF” method that can be used to improve the deconvolution of organic factors using atmospheric mass spectral data that don't have adequate mass resolution for unambiguous ion speciation. The authors applied this method to both ambient and synthetic data and demonstrated that the combination of mass spectral binning with positive matrix factorization is an effective approach to better resolve chemical information and to improve the separation of different sources and processes. This is an exciting new development in data analysis for real-time mass spectrometry and this work is of very high quality. The manuscript is very well written and the topic is a good fit for AMT. I thus recommend the manuscript be accepted for publication as is.

Response: We greatly appreciate this positive feedback on our work.

Anonymous Referee #2

This paper introduces a new method of interpreting ambient mass spectrometer data, binPMF. This is an extension of existing PMF techniques to sub-unity resolution mass spectra without the usual peak fitting stage before this. The advantage of this approach is that it can utilise the extra mass spectrometric information without having to specify the peaks that are expected to be present. I can foresee a number of applications for this technique; it could conceivably be used deliver more accurate factorisations than UMR-PMF, but I strongly suspect that it may prove more useful in identifying peaks to use for HR-PMF. However, time will tell on that. Presented as a proof-of-concept, this is likely to stimulate activity and further development within the community of users of ARI/Tofwerk instruments, but I would anticipate that this may have applications beyond this. The paper is certainly relevant to AMT and is very well written and presented. I have a few reservations (see below) but these are minor, so subject to these I recommend publication.

Comments: Generally, the authors are very bullish about the capabilities of the technique, but I can foresee a number of fundamental limitations. In the interests of properly exploring this method on a conceptual level, I would recommend that the authors discuss these so as to create realistic expectations of what this is capable of. The issues I can think of are as follows, but there may be others:

Response: We thank the reviewer for the comments and will answer them point-by-point below. We acknowledge already at this stage that our aim was not to present binPMF as a method without limitations. For example, any fundamental limitations inherent to PMF will obviously still apply to binPMF. Instead, we want here to emphasize the word “simple” in our title. HR fitting of spectra can be extremely laborious, and with enough ions at a single integer mass, HR fitting can become impossible. BinPMF can still be run in such cases, with data preparation requiring the same amount of work as for a simpler data set, informing the analyst about various aspects of his/her data, while still utilizing more spectral information than simply running UMR PMF.

* Peak shape - It must be explicitly stated that this technique assumes that the peak shape model is consistent throughout a dataset. While this should remain constant if the instrument is working properly, if it drifts somehow, then this will likely cause unpredictable behaviour here.

Response: For the technique of binPMF itself, it only tries to separate different bins based on their temporal behaviors, and the narrow bins help to preserve the high-resolution information. Thus, the technique does not assume anything about the peak shape. However, the reviewer is correct that in the way we present the results and their interpretation, we as analysts have assumed a constant peak shape throughout our data sets. Any variability in the peak shape, or resolution for that matter, will cause signal to “leak” different amounts into adjacent bins at different times. The larger this variation is, the harder the factor and peak separation becomes in binPMF.

An inconsistent peak shape in a data set will be a much larger issue for traditional peak fitting, and an invariable peak shape is a basic assumption in the routines of tofTools or Tofware. With problematic peak shape issues, only UMR results will be completely unaffected, but binPMF will be less affected, and thus likely provide a better result, compared to any method based on high-resolution peak fitting.

Ultimately, variable peak shapes over time are an indication that some large change has occurred in the instrument, and data before and after this change should likely not be analyzed together in the first place. Luckily, in our experience, the peak shape typically stays very consistent.

We added the following sentence (underlined) on Line 545-547 in Section 3.3 in the manuscript in order to briefly discuss this issue about peak shape:

“..... variation could also be considered for error estimation. Similarly, although generally rare and suggestive of some instrumental problem, if the peak shape or resolution shift over time, this would also require an improved error estimation in order to account for increased variability.”

* Aliasing - the act of binning the mass spectra through over- followed by under-sampling may introduce artificial smoothing of the data. This is unlikely to be an issue for peaks at low m/z ratios where the fundamental resolution of the instrument is high, but where the resolution of the mass spectrometer starts to become comparable to the target bin width, I imagine this could be an issue. This would be unlikely to cause problems if the mass calibration of the spectrometer were constant, but as this is known to subtly drift over time, this means that any aliasing artefacts could (in theory) be variable with time, even if the changes in calibration were properly accounted for, which in turn could create artificial factors in the dataset. This should be discussed, if only conceptually.

Response: In the binning process of binPMF, the data are first linearly interpolated with certain interpolation interval, and then binned with certain bin width. The bin width is much larger than the interpolation interval. The binning process considers all the interpolated data points within the bin width by averaging their signals, instead of just taking one data point as representative for this bin. In addition, in the manuscript section 3.3., we also suggest that the bin width should be mass-dependent and defined in such way that each peak can be covered by 7 bins, considering the instrument resolution (Th/Th).

While any resampling of data will inevitably lead to some smoothing, it should be minor with this approach. For the aliasing effect suggested by the reviewer, the fact that the bin widths are always clearly narrower than the peak widths, should make this effect negligible. We added a note on this into Section 3.3 on Line 516:

“Too few bins per peak would mean that we may lose valuable information in the binning, and potentially risk introducing aliasing effects, while too many points.....”

* Complexity - the analysis may not be able to adequately factorise systems where there is a large number of degrees of freedom in the chemistry, e.g. studying SOA formation in a chamber. This is a fundamental limitation of PMF and applies equally to the other established methods as well. However, I suppose this technique could still be of use in peak identification, even if it can't explain all the variance.

Response: Yes, we agreed with the reviewer that factorization analysis cannot separate every pathway/source. PMF itself, as a factorization analysis method, has its own fundamental limitations and problems and binPMF cannot improve on these problems. We added one sentence (underlined) in the manuscript in Line 173-174 in Section 2.1,

“.....considering their rotational uniqueness. Finally, we note that in addition to rotational ambiguity, binPMF also inherits all other fundamental limitations and strengths of the underlying PMF method.”

* Covariance - as with all PMF, the ability to separate components is contingent on them showing different trends. If (hypothetically) two adjacent peaks were to covary, then this technique would fail to separate them.

Response: Yes, the reviewer is correct. However, we do not find this to be a problem, and it would not impact the separation of factors.

Even so, for example, if there are $C_{10}H_{16}O_7$ and $C_9H_{12}O_8$ in the same mass spectrum, which will go to the same factor, we can still get the HR information in this factor, as it will now be a double peak at m/z of 310 Th in the factor. Thus, compared to UMR, we get more information. Compared to traditional HR fitting, assuming one knows the two ions are present at this mass, they can be fitted and separated, but will not contribute much more to the separation of different factors than the binPMF approach. In addition, if the two adjacent peaks are very close in mass, the attribution of signal between the two fitted peaks may become variable. This, in turn, may cause covarying ions to have different, anti-correlating behavior from improper HR fitting. This, again, highlights the robustness of binPMF, which requires no identification of ions beforehand, and is much less sensitive to variations in mass calibration, resolution or peak shapes.

Line 196: If the noise is based on signal-free regions of the mass spectrum, would this not be underestimated because of the thresholding applied by the data acquisition system?

Response: For the error estimation, we use this equation $S_{ij} = \sigma_{ij} + \sigma_{noise}$. The signal dependent part σ_{ij} represents the poisson counting error. The noise term σ_{noise} is to represent the background noise, stray counts etc. Exactly how good our method of noise estimation is, will depend on a wide variety of factors, including the frequency of ions measured at a given mass, the type of data acquisition card (compare e.g. TDC vs ADC), the ratio of the threshold level compared to the electronic noise, etc. . If the reviewer is suggesting that the electronic noise is “thresholded away” in the signal-free region, but that this noise is superimposed on the signal when an actual ion is detected, then there are a few effects counteracting this potential problem. At low count rates a given bin, most acquired spectra (sampled at ~10 kHz) will lack ions, and the majority of noise will arise from stray counts in the spectra, which were signal-free in reality. When the count rate becomes higher, the spectra with real signal become more dominant,

but at this stage the signal-dependent error term σ_{ij} will start to dominate the total error. In other words, for low (or no) signal bins, and for high signal bins, the error estimation approach is expected to work correctly. For intermediate count rates, there might be an effect as suggested by the reviewer. However, this cannot be addressed by simply increasing the noise term, since this would cause the low signals to have over-estimated noise. Thus, this simple error model is concluded to be adequate for the purpose of binPMF.

Line 535: I disagree that mass calibration could be accounted for by an error term; according to the PMF data model, the errors are supposed to be random and independent of one another, however a shift in mass calibration would cause deviations that are dependent on adjacent points.

Response: Uncertainty in PMF analyses arises from three main causes, as described in Paatero et al., 2014: (1) random errors in data values; (2) rotational ambiguity; and (3) modeling errors. This question by the reviewer is discussed in great detail in Paatero et al., 2014. Variations in mass calibration are one example of a modeling error. The assumptions underlying PMF are completely fulfilled if there are no modelling errors, and this is often the case in simulation studies. Then the results obtained from PMF obey rather strict mathematical rules, e.g. the Q contributions from individual columns or individual rows obey rather narrow chi-square distributions.

However, in real data, modeling errors are usually present, often in significant amounts. This means that statistical properties of PMF results are undefined. On the other hand, PMF analysis may still be used even in presence of modeling errors. It is common practice to include expected effect of modeling errors of data values so that the uncertainties S_{ij} specified for erroneous data values are artificially increased. In this way, the effect of modeling errors is constrained although it cannot be totally eliminated.

We added the following sentences in Line 536-544 in Section 3.3 in the manuscript,

“Uncertainty in PMF analyses arises from three main causes, random errors in data values, rotational ambiguity, and modeling errors (Paatero et al., 2014). Variations in mass calibration are one example of a modeling error, It is common practice to increase uncertainty values S_{ij} specified for data values disturbed by modeling errors. This increase does not account for the mass calibration error in the sense that the effect of mass calibration variation would disappear. The increase simply balances residuals in different data values so that the best possible result may be obtained. In addition to the two error estimation terms discussed in section 2.3, σ_{ij} and σ_{noise} , a third form of error, to balance the mass calibration variation could also be considered for error estimation.”

Reference

Paatero, P., Eberly, S., Brown, S. G., and Norris, G. A.: Methods for estimating uncertainty in factor analytic solutions, Atmos. Meas. Tech., 7, 781-797, doi:10.5194/amt-7-781-2014, 2014.

A Novel Approach for Simple Statistical Analysis of High-Resolution Mass Spectra

Yanjun Zhang¹, Otso Peräkylä¹, Chao Yan¹, Liine Heikkinen¹, Mikko Äijälä¹, Kaspar R.
Daellenbach¹, Qiaozhi Zha¹, Matthieu Riva^{1,2}, Olga Garmash¹, Heikki Junninen^{1,3}, Pentti Paatero¹,
Douglas Worsnop^{1,4}, and Mikael Ehn¹

¹ Institute for Atmospheric and Earth System Research / Physics, Faculty of Science, University of
Helsinki, Helsinki, 00140, Finland

² Univ Lyon, Université Claude Bernard Lyon 1, CNRS, IRCELYON, F-69626, Villeurbanne,
France

³ Institute of Physics, University of Tartu, Tartu, 50090, Estonia

⁴ Aerodyne Research, Inc., Billerica, MA 01821, USA

12

First author: Yanjun Zhang & Otso Peräkylä

Correspondence to: Yanjun Zhang (yanjun.zhang@helsinki.fi) & Chao Yan (chao.yan@helsinki.fi)

15

16

Abstract. Recent advancements in atmospheric mass spectrometry provide huge amounts of new information, but at the same time present considerable challenges for the data analysts. High-resolution (HR) peak identification and separation can be effort- and time-consuming, yet still tricky and inaccurate due to the complexity of overlapping peaks, especially at larger mass-to-charge ratios. This study presents a simple and novel method, mass spectral binning combined with positive matrix factorization ('binPMF') to address these problems. Different from unit mass resolution (UMR) analysis or HR peak fitting, which represent the routine data analysis approaches for mass spectrometry datasets, binPMF divides the mass spectra into small bins and takes advantage of PMF's strength in separating different sources or processes based on different temporal patterns. In this study, we applied the novel approach to both ambient and synthetic datasets to evaluate its performance. It not only succeeded in separating overlapping ions, but was found to be sensitive to subtle variations as well. Being fast and reliable, binPMF has no requirement for a priori peak information and can save much time and effort from conventional HR peak fitting, while still utilizing nearly the full potential of HR mass spectra. In addition, we identify several future improvements and applications for binPMF, and believe it will become a powerful approach in the data analysis of mass spectra.

Keywords. (Atmospheric) mass spectrometry, binned positive matrix factorization (binPMF), high-resolution (HR) mass spectra, peak fitting, chemical ionization mass spectrometer (CIMS), highly oxygenated molecules (HOM)

1. Introduction

Volatile organic compounds (VOC) are emitted to the atmosphere both from biogenic and anthropogenic sources (Guenther et al., 1995; Wei et al., 2008). After oxidation, these gaseous species can partition to the particle phase and contribute to atmospheric organic aerosol (OA), a major component of tropospheric particulate matter (Zhang et al., 2007). The chemical components, both in particulate (OA) and gaseous phase (VOC and their oxidation products), play important roles in many atmospheric physical and chemical processes. They can deteriorate air quality causing adverse health effects, and aerosol particles can influence Earth's climate by altering the radiative balance, as well as decrease visibility (Stocker et al., 2013; Zhang et al., 2016; Pope III et al., 2009; Shiraiwa et al., 2017).

47 Recent instrumental advances in mass spectrometry have greatly enhanced our capability to
48 investigate the chemical composition and evolution of aerosol particles and their precursors. The
49 Aerodyne aerosol mass spectrometer (AMS) is widely applied in atmospheric research (Canagaratna
50 et al., 2007), measuring the bulk composition and temporal behavior of the non-refractory aerosol,
51 and has successfully identified different/unique OA sources utilizing factor analysis (Jimenez et al.,
52 2009;Zhang et al., 2011). With the development of gas-phase chemical ionization mass spectrometry
53 (CIMS) (Huey, 2007), and the commercially available ToF-CIMS (Bertram et al., 2011) and CI-APi-
54 TOF (chemical ionization atmospheric pressure interface time-of-flight mass spectrometer (Jokinen
55 et al., 2012)), these instruments are becoming more popular in atmospheric chemistry research. Due
56 to these new advances, the detection methods for aerosol precursor vapors and the understanding of
57 their formation mechanisms have been greatly improved. For example, the discovery of highly
58 oxygenated molecules (HOM) by the CI-APi-TOF has led to increased knowledge regarding
59 atmospheric oxidation pathways, with large implications on secondary organic aerosol (SOA) and
60 new particle formation (Ehn et al., 2014;Jokinen et al., 2015;Kirkby et al., 2016;Yan et al., 2016). In
61 particular, biogenic VOC such as monoterpenes ($C_{10}H_{16}$), promptly produce HOM upon ozonolysis,
62 e.g. $C_{10}H_{16}O_7$ and $C_{10}H_{16}O_9$.

63 While a mass spectrum can contain large amounts of information representing the highly complex
64 nature of the atmospheric sample, it also presents considerable challenges for the analysis and
65 interpretation of the data. One example of such a challenge is the identification and separation of
66 peaks with a similar but not identical masses. A single integer mass can contain tens of distinct ions,
67 with mass-to-charge ratios (m/z) close to each other. In all cases, specific spectral fitting techniques
68 are needed to resolve the overlapping peaks at the same integer mass. Typically, a least squares fit is
69 made to the spectrum, using analysis software such as Squirrel/PIKA
70 (<http://cires1.colorado.edu/jimenez-group/ToFAMSResources/ToFSoftware/>), tofTools (Junninen et
71 al., 2010) or Tofware (<https://www.tofwerk.com/software/tofware/>). However, these techniques
72 require a pre-defined list of ions. This makes the analysis resource-intensive, and it can easily
73 introduce subjective bias in determining the peak list.

74 Figure 1 depicts a concrete example, measured by a nitrate-based CI-APi-TOF, where peak separation
75 is not large enough to allow unambiguous fitting of all the ions, and the final result will depend on
76 which ions the analyst chooses to include. As the m/z increases, the number of possible ions at a
77 certain unit mass increases rapidly (Kroll et al., 2011;Stark et al., 2015). Too closely overlapping
78 peaks will sometimes lead to ambiguously fitted peaks and arbitrarily resolved ions, resulting in
79 unreliable separation of signals. Additionally, mass calibration errors can also affect correct peak

80 assignment or fitting. A few recent studies discuss in more detail the uncertainties of ion identification
81 and separation in HR mass spectra (Stark et al., 2015;Corbin et al., 2015;Cubison and Jimenez, 2015).

82 Another typical analysis approach is to utilize only the unit mass resolution, or UMR data. As opposed
83 to high resolution fitting, where the signals of individual ions are separated from the total measured
84 signal, in UMR analysis all signals at a given integer mass is integrated and treated together. This
85 approach is more straightforward and less subjective than HR fitting, but loses all possible high
86 resolution details in the spectrum (see Figure 2).

87 Even with perfect high resolution peak fits, a spectrum typically contains information of hundreds, if
88 not thousands, of ions, many of which come from similar sources. This wealth of data itself presents
89 a challenge for data analysis. Factor analysis enables the reduction of data dimensions and can help
90 to apportion the signals to factors. These factors may correspond to different sources or formation
91 processes. Positive matrix factorization (PMF) (Paatero and Tapper, 1994) has been widely utilized
92 in environmental sciences, applied to UMR and HR AMS data, succeeding in identifying multiple
93 OA sources (Lanz et al., 2008;Ulbrich et al., 2009;Sun et al., 2011;Zhang et al., 2011). Compared to
94 AMS data, PMF has been applied to CIMS data analysis much less frequently. To our knowledge,
95 only Yan et al. (2016) and Massoli et al. (2018) have reported PMF analysis on nitrate-based CI-API-
96 TOF, utilizing UMR and HR data, respectively.

97 UMR-PMF cannot utilize the full information content provided by HR mass spectrometers, but is
98 more straightforward to apply. In contrast, accurate HR peak fitting can better preserve the
99 information content of the raw data than UMR, and thus provide more information to PMF, resulting
100 in more interpretable results. However, incorrectly fitted peaks can severely disturb the PMF
101 modeling and the factor interpretation. In addition, mass spectra from iodide-adduct Tof-CIMS (Lee
102 et al., 2014), often contain more peaks per mass than the NO_3^- -CI-API-TOF, making HR fitting much
103 more complex (or in some cases, even unmanageable), severely limiting the potential of HR PMF.

104 In this study, a novel, yet simple and reliable, data analysis method, binned mass spectra combined
105 with PMF (binPMF), is proposed to try to tackle the abovementioned problems in both HR and UMR
106 PMF. Instead of using traditional UMR or HR fitting techniques to the mass spectra, we binned the
107 mass spectra prior to PMF analysis (Figure 2). We applied binPMF to both ambient and synthetic
108 datasets, succeeding in separating the key components of different sources/processes. Compared to
109 UMR PMF, binPMF preserves more of the high resolution information content of the mass spectra,
110 without the immense effort and subjectivity associated with high-resolution peak fitting. As a result,

111 this novel method can improve our understanding of sources/formation processes governing the
112 particulate and gaseous phases in more detail and in a less subjective manner.

113 2. Methodology

114 We divided the mass spectra into narrow bins as presented in Figure 2, and carried out PMF analysis
115 to extract more information from the dataset. Details on the data preparation (binning the mass
116 spectra), and error estimation for the PMF input are discussed in the Sections 2.2 and 2.3. To test the
117 performance of binPMF under different scenarios, we first constructed synthetic datasets, using a
118 simple one-/two-mass system (Section 2.4.1). In the second step, we applied binPMF to an ambient
119 dataset measured with a NO_3^- -CI-API-TOF in a boreal forest site located in Southern Finland (Section
120 2.4.2).

121 2.1. Positive matrix factorization

122 The PMF model was developed by Paatero and Tapper (Paatero and Tapper, 1994) in the 1990s and
123 has been widely applied in the analysis of various types of environmental data ever since (Zhang et
124 al., 2017; Yan et al., 2016; Ulbrich et al., 2009; Song et al., 2007). By decomposing the observed
125 dataset into different factors, PMF helps to simplify the complex data matrix and extract useful
126 information contained within it. Compared to other common source apportionment tools, like
127 chemical mass balance (CMB) (Schauer et al., 1996), PMF requires no prior knowledge of source
128 information as essential input. Nevertheless, as a statistical method, PMF does require more data as
129 input, which is typically not a problem for environmental mass spectrometry datasets. The main
130 distinction of PMF from other factor analysis techniques is that PMF utilizes a least squares
131 minimization scheme weighted with data uncertainties, and non-negative constraints, to minimize the
132 ambiguity caused by rotation of the factors (Huang et al., 1999; Paatero and Tapper, 1994).

133 In PMF modelling, a measurement of chemical species is assumed to be a sum of contributions from
134 several relatively fixed sources/processes. The measured data matrix is broken down to two smaller
135 matrices, and a residual term as follows:

$$136 \quad X_{(m \times n)} = \text{TS}_{(m \times p)} \times \text{MS}_{(p \times n)} + R_{(m \times n)} \quad (1)$$

137 where X represents an $m \times n$ data matrix of original measurement for species n (e.g. m/z) at time point
138 m , TS is the $m \times p$ time series matrix of factor contributions, MS is the $p \times n$ matrix of factor profiles
139 or the factor mass spectra, and R is the residual between the modelled and the measured data. p is the
140 number of factors, which needs to be determined based on the interpretability of the PMF results,

141 among other criteria. Thus, in PMF, the original data matrix is approximated in terms of p factors,
142 each of which has a distinct mass spectrum and time series.

143 To find the solution, the PMF model utilizes uncertainty estimates for each element in the data matrix
144 X . These uncertainty estimates are used to weight the residuals (R), in order to calculate the Q value
145 as

$$146 \quad Q = \sum_{i=1}^m \sum_{j=1}^n \left(\frac{R_{ij}}{S_{ij}} \right)^2 \quad (2)$$

147 where S_{ij} is the estimated uncertainty of species/mass j at time point i , and R_{ij} is the residual of that
148 mass at the same time. Q is then minimized iteratively to find the mathematically optimal solution.
149 An expected Q value (Q_{exp}) can be calculated as the number of non-down-weighted data values in X
150 minus the sum of elements in TS and MS. If the data follows the requirements of PMF, the solution
151 with the correct number of factors should have a Q/Q_{exp} value near unity. When this is true, the
152 residuals on average fall within the expected uncertainties for each time point and variable. More
153 details about uncertainty estimation will be discussed in Section 2.3. The PMF analysis in this study
154 was performed with the toolkit of Source Finder (SoFi, v6.3) (Canonaco et al., 2013) by multi-linear
155 engine (ME-2) (Paatero, 1999). Masses with low signal-to-noise ratio ($SNR < 0.2$, see Section 2.3 on
156 error estimation) were down-weighted by a factor of 10, and masses with $0.2 < SNR < 2$ were down-
157 weighted by a factor of 2, as suggested by Paatero and Hopke (Paatero and Hopke, 2003). The down-
158 weighting effect was considered in the Q_{exp} calculation. In this study, PMF was operated in robust
159 mode, where outliers ($\left| \frac{R_{ij}}{S_{ij}} \right| > 4$) were dynamically down-weighted (Paatero, 1997).

160 One of the problems in any factorization analysis is rotational ambiguity, which is caused by an
161 infinite number of similar solutions generated by PMF (Paatero et al., 2002; Henry, 1987). Generally,
162 the non-negativity constraint alone is not sufficient for solution uniqueness. Rotating a certain
163 solution and assessing the rotated results is one possible way to determine the most physically
164 reasonable solution. Known source profiles or source contributions can also serve as constraints. In
165 addition, if there is a sufficient number of time points when the contribution of a source is nearly
166 zero, independent of other sources, rotational uniqueness of solutions can be achieved (Paatero et al.,
167 2002). The same is true if specific variables in the profiles go to zero. Otherwise, the correct solution
168 (correct rotation) may only be obtained by skillful use of rotational tools. Ambient measurement data
169 can often contain zero values in most sources/processes, greatly reducing rotational ambiguity of the
170 PMF results. The issue of rotational ambiguity is not explored in detail in this manuscript, as it is
171 common to all PMF approaches, and the main purpose here is to illustrate the new methodology of

binPMF. All the solutions shown in this study were achieved without considering their rotational uniqueness. Finally, we note that in addition to rotational ambiguity, binPMF also inherits all other fundamental limitations and strengths of the underlying PMF method.

2.2. binPMF data matrix preparation

Instead of UMR or HR fitting of the mass spectra, the mass spectra were divided into small bins after mass calibration (Figure 2 and Figure S1 in the Supplement). Data were first linearly interpolated to a mass interval of 0.001 Th, and then divided into bins of 0.02 Th width. At an integer mass N , only the signals between $N-0.2$ Th and $N+0.3$ Th (“the signal region”) were binned to avoid unnecessary computation of masses without any signal. With the binning, there were 25 data points for each nominal mass, instead of only one signal in UMR or several fitted peaks in HR analysis. All the parameters mentioned above, e.g. bin width and signal region size, should be adjusted to suit the mass spectrometer and the data being analyzed. Further details on binning procedures are discussed in Section 3.3.

2.3. binPMF error matrix preparation

Beside the data matrix, an error matrix describing the expected uncertainty for each element in the data matrix is also required as input in PMF analysis. Here, the error matrix (Polissar et al., 1998) is estimated as

$$S_{ij} = \sigma_{ij} + \sigma_{noise} \quad (3)$$

where the uncertainty of mass j at time point i , S_{ij} , is composed of analytical uncertainty σ_{ij} and instrument noise σ_{noise} . σ_{ij} is the uncertainty arising from counting statistics and is estimated as

$$\sigma_{ij} = a \times \frac{\sqrt{I}}{\sqrt{t_s}} \quad (4)$$

in which I is the signal intensity, in counts per second, t_s is the averaging time in seconds and a is an empirical parameter incorporated to include unaccounted uncertainties (Allan et al., 2003; Yan et al., 2016). In our study, we applied binPMF with CI-API-TOF data as an example, and the same a value of 1.28 was utilized as estimated previously from laboratory experiments in the work of Yan et al. (2016). The σ_{noise} is calculated as the median of the standard deviation of instrument noise, calculated from the bins between two nominal masses that should be least influenced by real signals (the noise region), i.e. $N+0.5$ - $N+0.8$ Th (see Figure S1 in the Supplement).

2.4. Data sources and description

201 This study utilized both ambient and synthetic datasets to test the performance of binPMF. The
202 ambient data was collected at the SMEAR II station (Station for Measuring Ecosystem–Atmosphere
203 Relations (Hari and Kulmala, 2005)) in the boreal forest in Hyytiälä, Southern Finland. Located in a
204 rural forest area, the station has a wide range of continuous measurements of meteorology, aerosol
205 and gas phase properties year-round. There are no strong anthropogenic sources close to the site, but
206 two sawmills 5 km to southeast and the city of Tampere 60 km to the southwest. Detailed
207 meteorological parameters and concentrations of trace gases during this campaign have been
208 presented earlier (Zha et al., 2018). Before the application to ambient data, we constructed a simple
209 synthetic dataset, to examine how well binPMF can separate overlapping ions under different
210 conditions.

211 **2.4.1. Synthetic dataset**

212 As a first test of the performance of binPMF, we generated a series of synthetic datasets based on two
213 distinct sources. Each synthetic dataset Y was created by summing up the signals of the two sources.
214 Each source consisted of a constant source profile (represented as the matrix MS), and had a unique
215 temporal behavior (represented as the matrix TS). Each source was the multiplication of MS (mass
216 spectra / source profile) and TS (time series). The two TS for the two sources were generated
217 randomly and independently from each other, as shown in Figure S2 in the Supplement (correlation
218 coefficient $R = 0.375$). To avoid rotational ambiguity (See section 2.1) in these tests, we added zero
219 values to the time series of the two sources, independently of each other.

220 As shown in Figure 3, each source profile (MS) was generated to consist of either one or two separate
221 peaks, covering either one or two unit masses, respectively. The peaks were generated as Gaussians
222 of known width and centroid position. The peaks of the different sources/profiles were partially
223 overlapping, with the exact overlap, i.e. the distance (m/z difference) between the overlapping peaks,
224 being varied from one experiment to another.

225 Peaks in the synthetic MS profiles were first generated as perfect smooth peaks (fine m/z interval of
226 0.00001 Th), with mass resolution of 5000 Th/Th. We define the resolution R of a peak as $R =$
227 $M/\Delta M$, where M is the mass of the ion, and ΔM is the full width at half maximum signal intensity,
228 FWHM. As an example, with $R = 5000$ Th/Th, an ion at m/z of 300 Th will have a FWHM of 0.06
229 Th, corresponding to 200 ppm. Multiplying the source profiles and the time series, we generated an
230 ideal data matrix. From this ideal matrix, we sampled with m/z interval of 0.015 Th to simulate the
231 real measurement data. The interval selected was close to that typically used for the HTOF mass
232 analyzer on a CI-APi-TOF. After the sampling, Gaussian distributed noise, both from background

random noise and signal dependent noise were added to make up the data matrix Y' , point by point, as shown in Eq. 6 below. The variance of the Gaussian distributed noise was estimated as one hundredth of the coefficient ' c ', which is the average value of Y .

$$Y = TS \times MS \quad (5)$$

$$Y'_{ij} = Y_{ij} + \text{Gaussian}(0, 0.01 \times c) + \text{Gaussian}(0, 1) \times \sqrt{Y_{ij}} \quad (6)$$

Finally, random m/z shift within ± 10 ppm was added to simulate mass calibration error, spectrum by spectrum. This error, resulting from inaccurate conversion of the time-of-flight into mass-to-charge ratio, is one of the main causes of ambiguous or incorrect peak assignment or fitting. In our study, with the bin width of 0.02 Th and the mass calibration error of 10 ppm, a maximum of 15% of one bin's signal may incorrectly shift to the adjacent bin, for a mass at 300 Th ($(10 \text{ ppm} \times 300 \text{ Th}) / 0.02 \text{ Th} \times 100 \% = 15\%$). The impact of this mass shift will effectively be smaller, due to the high temporal correlation of adjacent bins, as the signal from an ion will spread to several adjacent bins (the FWHM is ~ 3 times the bin width). In the case of HR fitting of peaks, a 10 ppm mass calibration error may cause much more dramatic changes than merely shifting 15% of the signal. There is also no reason for ions from a given source to selectively end up at the same integer mass, meaning that the signal is likely to be shifted to another ion from a completely different source.

Twenty-one synthetic experiments were designed, varying the mass difference between peaks (m/z difference) and number of unit masses included in the MS, as shown in Table S1 and Figure 3. For experiments 1-10, each of the two source profiles consisted of one peak (A1 and B1), both located at the same unit mass (chosen to be 310 Th in this study), with varying separation of the peak centroids. In experiments 11-20, we added one more peak to each profile (peaks A2 and B2), in addition to peaks A1 and B1. The additional peaks were added at another unit mass (311 Th) and their m/z difference was fixed at 0.05 Th (161 ppm), while the position of peak B1 was varied as in experiments 1-10. For experiment 21, peaks A2 and B2 were added at two different masses (311 Th and 312 Th), corresponding to a m/z difference sufficiently large that there was no meaningful overlap between them. In the MS (i.e. mass spectra profiles), all peaks had the same intensity level initially. The variation of the peak intensity ratio comes from variations in the time series (Figure S2 in Supplement). The same time series for each of the two sources was used in all experiments 1-21.

With this approach of only using two masses, we purposefully provide a challenging dataset for binPMF, as in most real datasets there would be many more masses to help to constrain the final solutions. Nevertheless, as we will show, this simple synthetic dataset already provided a wealth of

264 useful information in the results attainable with binPMF, and provided a good comparison to the
265 traditional HR fitting approach.

266 2.4.2. Ambient dataset

267 The ambient dataset was measured at ground level during the Influence of Biosphere-Atmosphere
268 Interactions on the Reactive Nitrogen budget (IBAIRN) campaign (Zha et al, 2018) in September,
269 2016. The measurements were conducted using a NO_3^- -CI-APi-TOF that has been described in detail
270 elsewhere (Jokinen et al., 2012; Junninen et al., 2010; Yan et al., 2016). Here, the ambient gas-phase
271 molecules clustered with the nitrate ion were measured with about 4000 Th/Th mass resolving power.
272 Data from September 1st to 26th, averaged to 1-hour time resolution, in the mass range of 300 - 350
273 Th (a typical monoterpene HOM “monomer” range, Ehn et al., 2014) were utilized for the binPMF
274 analysis. A baseline subtraction was applied to the mass spectra, which caused some small signals
275 next to large peaks to become negative. In our analysis, any m/z bin where the median signal was
276 negative was excluded from the data matrix.

277 3. Results and discussion

278 3.1. Synthetic dataset

279 3.1.1. Experiment settings

280 As introduced in Section 2.4.1, the synthetic datasets were constructed to assess the response of
281 binPMF to varied m/z difference, peak intensity ratios, and number of masses included, as shown in
282 Table S1 and Figure 3. The smaller the distance between the two peaks, the harder it is to accurately
283 separate them with traditional HR peak identification and fitting. In our experiments, the m/z
284 difference was decreased stepwise from 0.050 Th (161 ppm) to 0.001 Th (3 ppm), in a system where
285 the FWHM was roughly 200 ppm.

286 The analysis procedure of the synthetic dataset is briefly described here. In all cases, the parameter
287 of interest is to see how well binPMF is able to deconvolve the adjacent peaks A1 and B1 at m/z 310
288 Th. First, binPMF was applied to the synthetic datasets, and factors profiles (mass spectra) were
289 extracted. The optimal number of factors for the synthetic dataset is two, the same as the number of
290 sources, so only the two-factor solution was studied with binPMF. The results of the diagnostic
291 parameter Q/Q_{exp} for each experiment are included in Table S1. Gaussian fitting was then performed
292 on the factor profiles to retrieve the locations of peaks A1 and B1, and thereby assess how well
293 binPMF was able to retrieve the original peak positions.

294 In addition to applying binPMF to the synthetic datasets, traditional HR peak fitting was also
295 conducted as comparison (by tofTools in our study). For the tofTools fits, we constrained the peak
296 locations and widths to those originally used for generating the data (Table S1). Peaks fitted by
297 tofTools and peaks fitted to the binPMF factors were compared, as well as the retrieved time series
298 correlation with the original datasets. More details are presented and discussed in the following
299 sections.

300 3.1.2. Comparison of peak fitting

301 We examined the performance of traditional HR fitting and binPMF by comparing their results to the
302 original input data. In Figure 4, the shaded areas depict the original data, the dashed lines the
303 traditional HR peak fitting result, and the solid lines the binPMF factors. Red and blue represent
304 source/factor A and B, respectively. Panels a-d (in Figure 4) show four scenarios of peak fitting results
305 from experiments 1, 5, 10 and 20, at the 79th time point, where the two peaks had similar signal
306 intensities. When the two peaks were separated by 0.05 Th (Figure 4a), both methods captured the
307 peak intensities quite well. However, as the m/z difference narrowed, the performance of both
308 methods declined, with the HR fitting results deteriorating faster than those from binPMF. As m/z
309 difference reached 0.001 Th (3 ppm), the traditional HR fitting method completely failed to fit the
310 two peaks (panels c and d), instead attributing all the signal to just one fitted mass. In panels e-h, the
311 peak fitting results at the 21st time point are displayed, where the ratio of the two peaks was roughly
312 1:6. Here, the traditional fitting method failed to extract the two peaks already at a m/z difference of
313 0.01 Th (30 ppm), attributing all signal to Peak B1 (panels g and h). As shown in panels d and h,
314 when a second set of peaks, separated by 0.05 Th, was introduced for the two sources in the datasets,
315 binPMF was able to utilize the temporal behavior of peaks A2 and B2, performing much better, even
316 in the extremely difficult cases when the m/z difference for the two peaks was only 0.001 Th (3 ppm).
317 It is an inherent advantage of binPMF over traditional peak fitting methods that the temporal behavior
318 and the correlations between different variables can be utilized.

319 Figure 5 shows an overview of all the results of peaks fitted with binPMF. Experiments 1-10 for the
320 one-mass system are shown with green lines, and experiments 11-20 for the two-mass system in
321 yellow. Mass accuracy was calculated as the difference between fitted peak center mass and the
322 original mass, divided by the original mass, in ppm. When the m/z difference got smaller, the mass
323 accuracy of peaks fitted to binPMF factors declined (Figures 5a and 5c). At a m/z difference of 0.01
324 Th (32 ppm), the mass accuracy was -4 ± 2 ppm and 7 ± 2 ppm for peaks A1 and B1, respectively. The
325 uncertainties were estimated by repeating the analysis with 10 different random time series for the
326 two sources (Brown et al., 2015). For comparison, this separation approximately corresponds to that

327 between $\text{C}_{10}\text{H}_{16}\text{O}_7\cdot\text{NO}_3^-$ (310.0780 Th) and $\text{C}_9\text{H}_{16}\text{N}_2\text{O}_6\cdot\text{NO}_3^-$ (310.0892 Th). With m/z difference
328 decreasing, the position of peak A1 (the left red peak in Figure 3), as identified by binPMF, shifted
329 gradually to the left, while peak B1 (the right blue peak) shifted to the right. When peaks A2 and B2
330 were introduced to the sources, the mass accuracy improved (< 6 ppm). The resolution of the peaks
331 fitted to binPMF factor profiles stayed fairly constant, but had degraded compared to the original
332 input data (5000 Th/Th), explained at least partially by the data binning (Figures 5b and 5d). Overall,
333 binPMF performs relatively well in peak separation, with reasonable mass accuracy and peak
334 resolution compared to the original datasets.

335 3.1.3. Correlation of time series

336 In addition to the peak positions, we also compared the temporal behavior of both the binPMF factors
337 and the time series obtained through traditional fitting, to the original time series. When m/z difference
338 was larger than 0.02 Th (65 ppm), both methods worked similarly well in reproducing the original
339 time series (Figure 6). As the m/z difference decreased below 0.02 Th (65 ppm), correlations
340 decreased rapidly (panels a and c), with that of the traditional method decreasing faster. However, as
341 shown by the yellow lines, when peaks A2 and B2 were added to each source profile, the time series
342 correlation coefficients between original data and peaks extracted by binPMF were close to unity in
343 experiments 11-20. The coefficients stayed similar to that from the experiment with m/z difference of
344 0.05 Th (161 ppm), which was the fixed m/z difference for the two new peaks added at 311 Th in
345 experiments 11-20. This means that the separation of the factor time series was mainly driven by the
346 additional, better separated peaks. Again, the traditional HR fitting method could not utilize the
347 information at 311 Th, and therefore no improvement to the peak deconvolution at 310 Th was seen.
348 In addition to the correlation analysis, also the assignment of absolute signal to peaks A1 and B1 was
349 evaluated. This was done by a linear fit (through zero) to the data points retrieved by the different
350 methods as a function of the original input data. The slopes of the fitted lines are plotted in Figures
351 6b and 6d, and show that the signal was for the most part correctly attributed to within a few percent.
352 The largest scatter in the determined slopes were observed for binPMF experiments with only one
353 mass, at low peak separations.

354 3.1.4. Summary and discussion

355 Based on the results shown above, binPMF was found to be as capable of separating different peaks
356 as traditional peak fitting techniques when the two peaks were separated by more than the mass
357 calibration uncertainty (yet still in all cases by less than the FWHM of the peaks). As the m/z
358 difference of the two overlapping peaks decreased, the performance of the traditional method declined

359 faster than that of binPMF. This was shown for signal attribution of fitted peaks and time series
360 correlation with original data. When masses with co-varied temporal behavior of the targeted
361 overlapping peaks were introduced in the dataset, the performance of binPMF improved significantly.

362 The peak fitting principle of the traditional method and binPMF are very different. For example,
363 tofTools fits peaks based on pre-determined instrument parameters (e.g. peak shape and peak width),
364 as well as the peak location, either as a numeric value, or a chemical composition from which the
365 location is calculated (Junninen et al., 2010). HR peak fitting by tofTools can be effective if the
366 majority of the components (peaks) are known and provided in a peak list, which is valuable
367 information for peak separation that was not provided to binPMF in this study. However, this
368 information can be hard to achieve due to unknown numbers and/or identities of all the ions at a given
369 mass, in combination with the limited mass resolving power of the mass spectrometer. HR peak fitting
370 is also sensitive to mass calibration error, increasingly so when many ions in close proximity to each
371 other need to be fit. On the contrary, in binPMF, peaks are separated based on the temporal variation
372 of masses, which is an inherent advantage of PMF, though no information of the peaks is provided
373 beforehand. To be more specific, a conceptual illustration is shown in Figure S3 in the Supplement.

374 The red peaks belong to Source A and the blue peaks to Source B. As mentioned before, the time
375 series of sources A and B were totally independent and random. The shaded areas (the tails of the
376 peaks), e.g. red shaded area in Figure S3a, contained masses that only had significant signal from
377 peak A1 (left red peak). Similarly, the blue shaded area in Figure S3a was mostly from peak B1. The
378 different temporal behaviors of the red and blue shaded areas helped the separation and correct
379 attribution also in the regions with overlapped signals. When the m/z difference of peaks A1 and B1
380 decreased, shown in Figure S3b, the two shaded areas also became smaller. This is the main reason
381 why the fitted masses of binPMF had lower mass accuracy and lower correlation coefficients
382 compared to the original data, as the m/z difference decreased.

383 When peaks A2 and B2 (m/z difference of 0.05 Th) were added in the dataset, peaks A1 and B1 were
384 better separated and fitted by binPMF compared to the scenarios with only one mass. This is because,
385 as shown in Figure S3c, the red and blue shaded areas became larger due to the addition of two more
386 peaks. In this case, it was peaks A2 and B2 that dominated the separation of sources A and B. In
387 experiment 21, three integer masses were included in the dataset. Though it was still equally difficult
388 for the traditional HR method to separate and fit peaks A1 and B1 with m/z difference of 0.001 Th (3
389 ppm), it was the easiest experiment for binPMF out of all the experiments because of the large m/z
390 difference of peaks A2 and B2 (1.000 Th, 3225 ppm). In experiment 21, the mass accuracies for peaks
391 A1 and B1 were -3.2 ppm and 2.6 ppm, respectively, and the time series correlation with original data

392 was 1.000 and 0.999, respectively. In most real-world applications, individual sources typically
393 contain multiple peaks, and the correlations of these can be utilized by binPMF.

394 We note once more that the results of binPMF and traditional HR peak fitting are not totally
395 comparable. Information about the peaks, like the exact peak centroid position, peak width
396 (resolution) and number of peaks, was provided to the traditional fitting method. For binPMF, no
397 prior information about the peaks was given, except for the optimal number of factors, i.e. two.

398 **3.2. Ambient dataset**

399 With the success of binPMF for the synthetic datasets, we applied the new method to a real ambient
400 dataset. Here we used data collected in September 2016, from Hyytiälä in Finland. The SMEAR II
401 station is a forest site dominated by monoterpene ($C_{10}H_{16}$) emissions (Hakola et al., 2006). Previous
402 CI-API-TOF measurements of HOM at the site (Ehn et al., 2014; Yan et al., 2016) have presented
403 bimodal distributions, with one mode corresponding to HOM monomers (range 300-400 Th) and the
404 second to HOM dimers (450-650 Th). For testing the binPMF analysis on our ambient dataset, we
405 selected the HOM monomer range of 300-350 Th. While the synthetic dataset primarily compared
406 binPMF to traditional HR fitting analysis, in this section, we compare the binPMF results with that
407 of traditional UMR-PMF, as employed by Yan et al. (2016). HR fitting was not performed for the
408 ambient dataset, for all reasons mentioned in earlier sections, including the difficulty and efforts of
409 producing a proper unambiguous peak list, as well the limitations of overlapping peaks.

410 As mentioned above, no prior knowledge was provided to PMF before the analysis. To determine the
411 number of factors for further analysis, we conducted runs with two to eight factors. As the number of
412 factors increased, more information could be extracted from the raw data. However, after the optimal
413 number of factors, the additional factors may split the physically reasonable factors into meaningless
414 fragments. There has been many studies on evaluations of PMF runs and selections of PMF factor
415 number (Zhang et al., 2011; Craven et al., 2012). This is an inherent challenge in any PMF analysis,
416 and not specific to binPMF, and therefore we do not put emphasis on this here. In this study, based
417 on commonly used mathematical parameters and physical interpretation, we chose the seven-factor
418 result, as presented below. Our main aim with this work is to present a ‘proof of concept’ for the
419 binPMF methodology, and we will therefore not provide a detailed interpretation of all the factors
420 (though several of the factors are easily validated based on earlier studies). The factor evolution from
421 two to eight factors are briefly discussed below.

422 From two to six factors, Q/Q_{exp} showed a dramatic decrease from 6.5 to 2.7. Then for seven and eight
423 factors, Q/Q_{exp} decreased to 2.3 and 2.0, respectively. The unexplained variation also declined from

14% to 8.8% going from two to six factors, then reached 8.0% for seven factors, and 7.6% for eight factors. The two-factor solution first split the data into a daytime factor and a nighttime factor, with very distinct mass spectral profiles. The daytime factor was characterized by signals at 307 Th, 311 Th, 323 Th, 339 Th and other odd masses, while the nighttime factor was dominated by 308 Th, 325 Th, 340 Th and 342 Th. The odd masses are typical signatures of day-time monoterpene-derived organonitrates at the site, while the even masses, and specific odd masses e.g. a radical at 325 Th, have been identified as monoterpene ozonolysis products (Ehn et al., 2014; Yan et al., 2016). As the number of factors increased, the daytime factor was further split into new daytime factors, with diurnal profiles having various peak times around noon or early afternoon. When the number of factors increased to seven, a clear sawtooth shape in the diurnal trend was resolved with marker masses at 308 Th, 324 Th, 325 Th, and 339 Th. Many of the profiles resolved in the seven-factor solution are similar to those found by Yan et al. (2016), and separating more factors did not yield new factors that we could interpret. Therefore, we opted to use this seven-factor result for the main discussion below, as it provided us with enough information to evaluate the binPMF method for this dataset.

Figure 7 shows the mass spectral profiles and factor time series for the 7-factor result, while Figure 8 displays the diurnal trends and factor contributions to the total signal. As shown in Figure 8a, the seven factors separated by binPMF consist of one nighttime factor (Factor 1), five daytime factors (Factors 2, 3, 4, 5 and 7) and a sawtooth-pattern factor (Factor 6). The same dataset was also analyzed by UMR-PMF, and the corresponding seven-factor results are also included in Figures 7 and 8 for comparison.

Overall, the results between UMR-PMF and binPMF are very similar. UMR-PMF also resolved one clear nighttime factor, and additionally six daytime factors. For the nighttime factor, both binPMF and UMR-PMF showed comparable temporal behavior, diurnal trend (peak at 17:00), mass spectral profiles (peaks at 340 Th, 308 Th, 325 Th, 342 Th) and factor contribution (~ 20%). This factor has been validated in both chamber and ambient studies to be formed from monoterpene ozonolysis (Ehn et al., 2014; Yan et al., 2016). As shown in Figure 7a, both methods also resolved similar, though not identical, mass spectral profiles for the other six factors, with mostly comparable time series (Figure 7b) and peak times in the diurnal trends (Figure 8a).

Despite the similarities, there also existed distinct differences between the results from binPMF and UMR-PMF. As the most distinctive dissimilarity, binPMF Factor 6 revealed a “contamination factor”. This factor was found to be related to automated instrument zeroing every three hours, giving rise to the distinct three-hour sawtooth pattern. The ~~zero measurements had been removed from the~~

457 ~~data matrix, but the~~ zeroing system introduced some additional compounds into the sampling lines,
458 and the semi-volatile nature of these compounds caused them to linger, and slowly decay, in the
459 tubing even after the instrument had returned to sampling ambient air. binPMF accurately retrieved
460 the 3-hour interval of the zero measurements. However, with the same mass range (300-350 Th),
461 UMR-PMF failed to extract the contamination factor, regardless of the number of factors retrieved
462 (up to 20 factor solutions were evaluated). Instead, these contamination signals were always mixed
463 into the other factors. Factor 6 from UMR-PMF contributed almost twice as much as that estimated
464 by binPMF due to the inaccurate factor separation (Figure 8b). The time series of other factors, e.g.
465 Factors 5 and 7 in UMR-PMF, were clearly influenced by Factor 6. Compared to UMR-PMF, binPMF
466 thus showed a clear advantage in providing more information out of the data by being more sensitive
467 to subtle variations.

468 In addition to better resolving certain factors from the data, the binPMF mass spectral profiles will
469 still contain more information than visible in Figure 7, due to the multiple bins at each unit mass. As
470 an example, binPMF Factor 6 showed masses with clear negative mass defects, e.g. at 324 Th and
471 339 Th (Figure 9). We identified many ions in this factor as different fluorinated carboxylic acids,
472 common interference signals in negative ion CIMS, outgassing from e.g. Teflon tubing (Brown et al.,
473 2015;Ehn et al., 2012;Heinritzi et al., 2016). The exact source of these products in our setup was not
474 established, but it is not surprising that the additional valves, filters and/or tubing in the zeroing line
475 could have caused this type of signal to be introduced to the instrument with the zero air. In general,
476 this finding highlights the usefulness of the binPMF approach, where factor separation can be
477 performed first, and the specific factor profiles can be utilized in interpreting the physical meaning
478 of the different factors. This is in complete contrast to the more traditional approach, where all ions
479 need to be identified first, and only then can HR PMF be attempted. As not all ions are going to be
480 observable at all times, many ions may remain unidentified. For example, if peak identification would
481 only have been done during periods when the HOM signals were high, as in the case shown in Figure
482 9a, the fluorinated ion at 339 Th would not have been found (contributing only 0.45% to the total
483 signal at this time point), even though it on average contributes nearly 10% of the signal at this mass
484 over the entire campaign. binPMF, on the other hand, utilized the full dataset for the identification,
485 and was able to separate several ions at 339 Th. By fitting gaussian signals to the factor profiles,
486 similar to the synthetic data in section 3.1.2, we see that the two major peaks were fitted with decent
487 resolution (Figure 9). Also the contamination factor (Factor 6) was clearly separated and fitted, and
488 the resolution (3136 Th/Th) is slightly underestimated by the fit, as only one gaussian was fitted to
489 each profile, yet there are clearly more than one ion at 339 Th in Factor 6. As shown in Figure 9c,

there is also clear indication that Factors 3 and 5, which together make up as much signal at 339 Th as the contamination Factor 6, mainly contain signals from another molecule ($C_{10}H_{13}O_9$) than the dominant signals at this mass ($C_{10}H_{15}NO_8$). However, further work will be needed to validate this. Factor 1 has marginal contribution to the signal at 339 Th (as seen in Figure 9b) throughout the campaign, and we expect it does not contain useful signal, as is suggested by the unreasonably high resolution, i.e. narrow peak width, of the fitted peak. The resolving power of the instrument was around 4000 Th/Th, and thus any apparent peak resolution above that will be unrealistic. However, as this factor contains signal at the outer edges of the main peaks at this m/z , it is possible that this factor relates to some instrumental variability affecting the peak shape. This is highly speculative, but such a phenomenon may be worth looking into in later studies utilizing binPMF. In summary, resolving multi-overlapping peaks by traditional methods is time-consuming and can be tricky and ambiguous. Here, binPMF greatly simplified this problem, by providing additional separation between the ions.

3.3. Future improvements and applications

The new technique for mass spectra analysis, binPMF, as presented above, shows clear promise in utilizing HR information while saving time and effort, as well as decreasing ambiguity related to conventional HR peak fitting. It is also more sensitive to subtle variation than standard UMR analysis. We consider this study a succesful proof-of-concept, and note that several future improvements and applications are still foreseeable. We list some of these below:

(1) **Varied bin width.** The full width at half maximum of an individual peak in a mass spectrometer is mass dependent, with peaks getting wider at higher masses. In binning the mass spectrum with a constant bin width, like in this study, the average number of bins per peak increases as a function of mass. To represent the peaks in a comparable manner, the bin width should thus be dependent on the mass. Varying the bin width as a function of the mass, and the mass resolution of the instrument, would enable a constant number of bins (e.g., seven) per peak. Too few bins per peak would mean that we may lose valuable information in the binning, and potentially risk introducing aliasing effects, while too many points per peak would lead to an unnecessarily high number of variables, without noticeable gain in information content. This would also result in high computational cost. If targeting 7 bins per peak, then the function for determining bin width based on m/z and resolution (R , which is mass-dependent) could be

$$\therefore R(m/z) = \frac{m/z}{\Delta m}$$

$$Bin\ width \times 7 = 2 \times \Delta m$$

$$\therefore Bin\ width = \frac{2}{7} \times \frac{m/z}{R(m/z)}$$

Δm is the full peak width at half maximum signal intensity. If we consider an instrument with approximate constant resolution of 5000 Th/Th for masses from 200 Th to 600 Th, the bin width at 200 Th and 600 Th should be around 0.01 Th and 0.03 Th, respectively.

- (2) **Optimization of binning region.** Similarly to bin width, the binning region, i.e. the signal region ($[N-0.2, N+0.3]$ in this study, introduced in section 2.2), should also be mass-dependent. Due to the widening of the peaks with increasing mass, the binning region should also get wider. In addition, the typical mass defect of measured ions typically varies with mass. This means that the binning regions should not necessarily be defined with respect to the integer masses, but to some chosen mass defect. Another approach would be to bin all the data, and remove the bins not meeting a certain criterion, such as one related to the signal to noise ratio in that bin, afterwards. In this case, there would be no need for a pre-defined mass defect or region width, and one could utilize the signals that do not fall within the expected regions.

- (3) **Error estimation.** Good error estimation is crucial to PMF calculation. Uncertainty in PMF analyses arises from three main causes, random errors in data values, rotational ambiguity, and modeling errors (Paatero et al., 2014). Variations in mass calibration are one example of a modeling error. It is common practice to increase uncertainty values S_{ij} specified for data values disturbed by modeling errors. This increase does not account for the mass calibration error in the sense that the effect of mass calibration variation would disappear. The increase simply balances residuals in different data values so that the best possible result may be obtained. In addition to the two error estimation terms discussed in section 2.3, σ_{ij} and σ_{noise} , a third form of error, caused by to balance the mass calibration variation could also be considered for error estimation.Similarly, although generally rare and suggestive of some instrumental problem, if the peak shape or resolution shift over time, this would also require an improved error estimation in order to account for increased variability.

- (4) **Multi-peak fitting.** As discussed, peak identification is one of the most time-consuming and potentially ambiguous tasks in HR analysis, and with binPMF this may not always be a necessary task. However, as binPMF often resolves several peaks (chemical components) at each integer mass, peak identification can be made easier if peak identification is constrained to several binPMF factor profiles rather than just the initial HR spectrum. The optimal approach for this will be the target of a future study.

Most likely several other improvements to the approach will be identified in future studies, and simplicity of the analysis remains a critical consideration. We propose that binPMF is a good tool for initial exploration of new datasets, at which stage optimizing all parameters is not necessarily crucial, if the results can help guide further analysis directions. However, for maximizing the information content that can be extracted from a given data set, optimized routines are important.

4. Conclusions

While recent advances in mass spectrometry have greatly enhanced our understanding of atmospheric chemistry, the increased information content in mass spectra also brings difficulties and challenges to the data analysis. Peak identification and separation can be challenging and ambiguous, as well as extremely time-consuming and involving large uncertainties. Constructing peak-lists, i.e. deciding which ions to fit to the mass spectra, and validating the results is becoming one of the most labor-intensive parts of the entire work. In this study, we propose a simple and reliable method, binPMF, to try to avoid many of these problems, while still being able to distinguish different chemical pathways/sources in the atmosphere.

Different from traditional analysis, binned positive matrix factorization (binPMF), divides the mass spectra into smaller bins, before applying PMF to distinguish different types of factors and behavior in the data. This method utilizes more available information than classical UMR-PMF, and requires no prior peak information as in the case of traditional HR-PMF. We applied binPMF successfully to both ambient and synthetic datasets to test its usefulness under different circumstances.

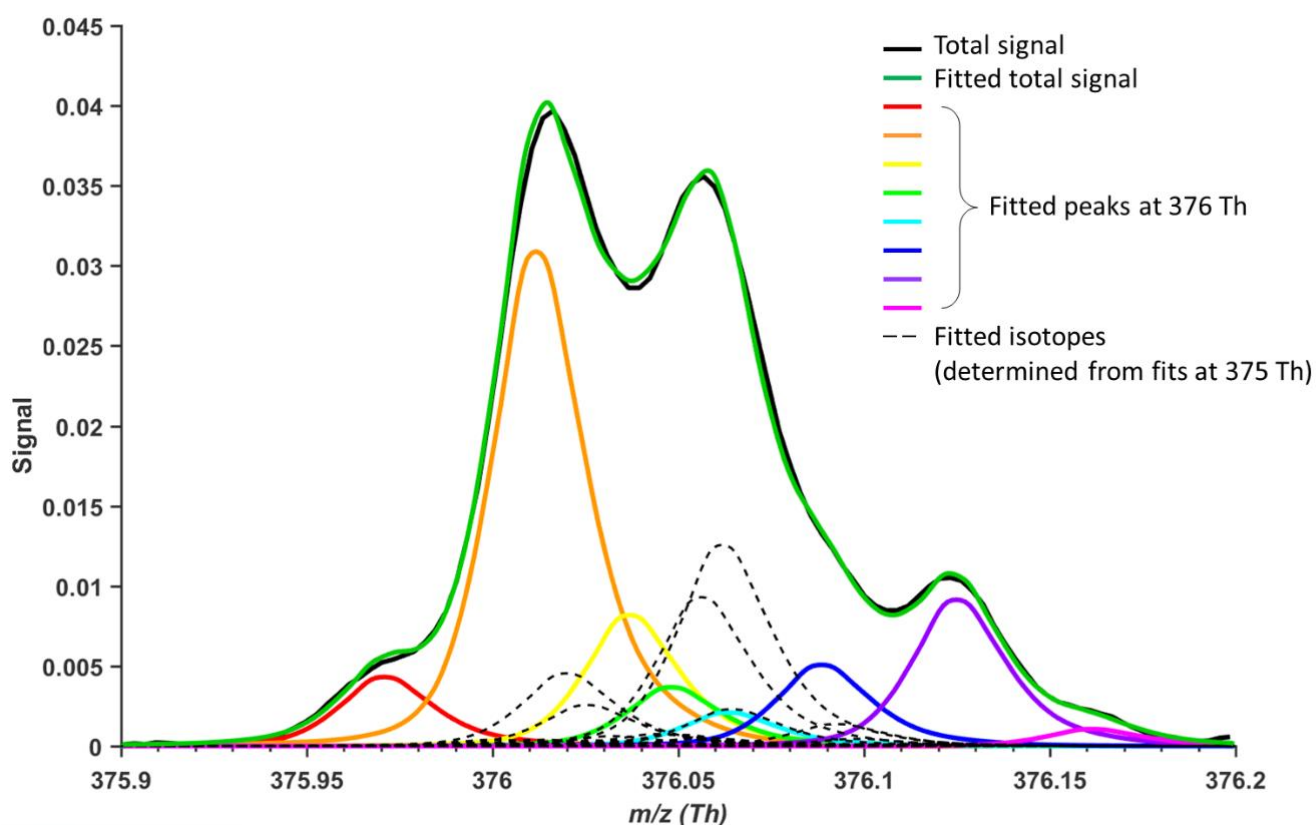
Traditional HR analysis fits peaks to each mass according to a pre-defined list, and is not able to utilize any information across masses or time. In our analysis of a simple synthetic data set with two overlapping ions at a single integer mass, we found that binPMF was able to separate the contributions of each ion even in cases where the HR analysis failed completely. This was the case for overlapping ions where binPMF had help in constraining the time series from another integer mass. When applied to an ambient dataset of HOM measured by a CI-API-TOF, binPMF identified more physically meaningful factors than UMR-PMF. Additionally, for factors where the two PMF approaches agreed, binPMF still contained more mass spectral information for ion identification, as compared to UMR-PMF.

We provide a proof-of-concept for the utility of binPMF, showing that it can outperform the two traditional analysis approaches, UMR and HR. We identify several future improvements and applications for binPMF, including an approach to greatly facilitate the time-consuming process of peak-list construction. We expect binPMF to become a powerful tool in the data exploration and analysis of mass spectra.

587 **Acknowledgements**

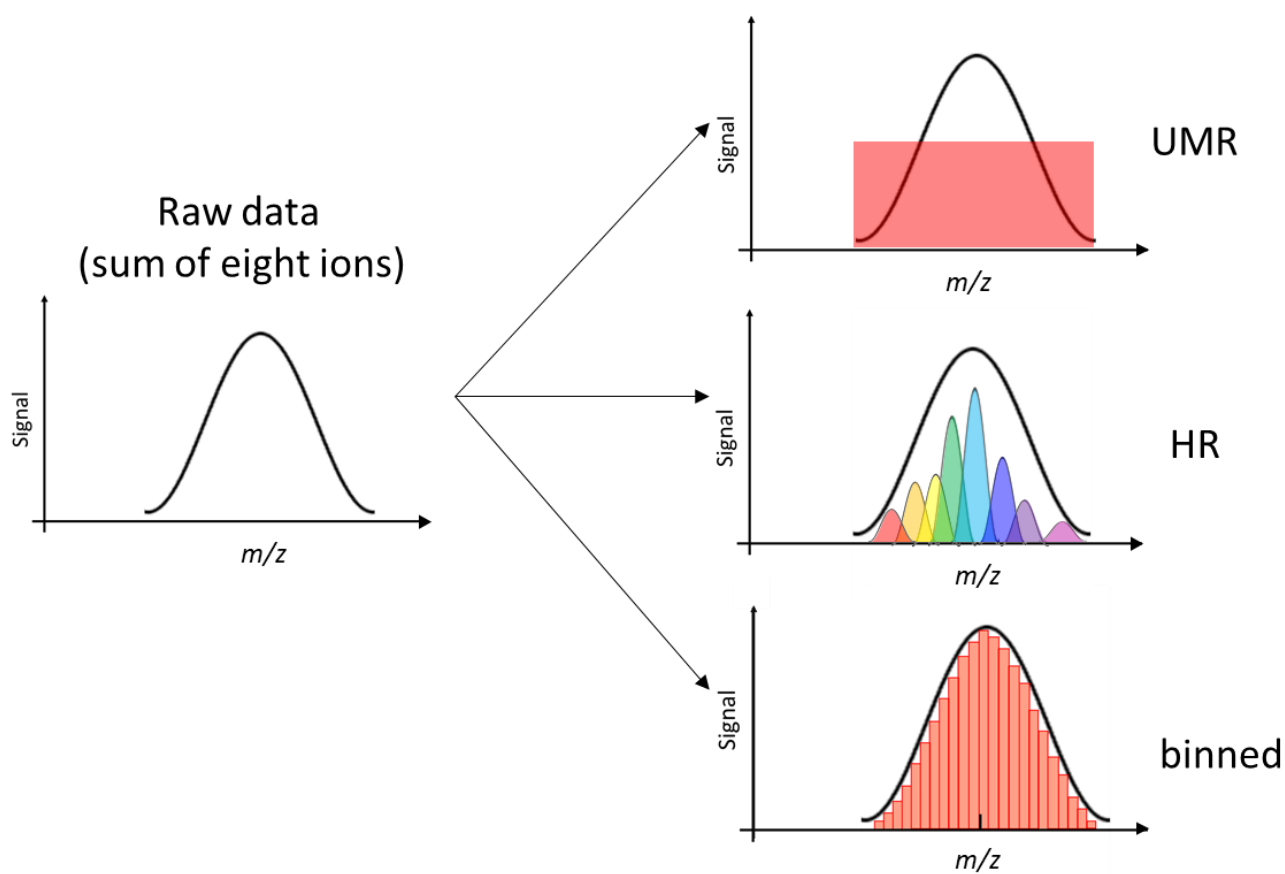
588 This research was supported by the European Research Council (Grant 638703-COALA), the
589 Academy of Finland (grants 317380 and 320094), and the Vilho, Yrjö and Kalle Väisälä Foundation.
590 K.R.D. acknowledges support by the Swiss National Science postdoc mobility grant
591 P2EZP2_181599. We thank the tofTools team for providing tools for mass spectrometry data
592 analysis. The personnel of the Hyytiälä forestry field station are acknowledged for help during field
593 measurements.

594



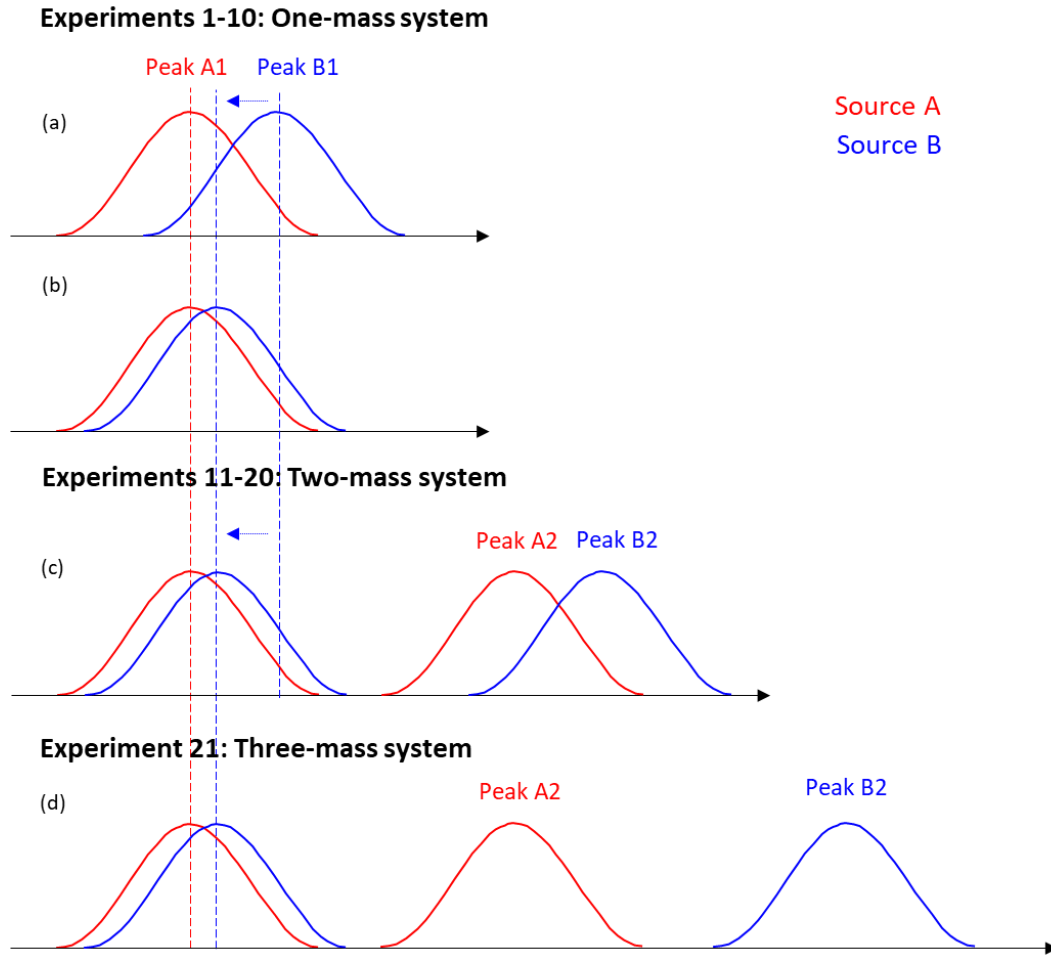
595

596 Figure 1. Example of traditional HR peak fitting. Potential peak fitting at m/z 376 Th (10-h average)
 597 in an atmospheric simulation chamber during a monoterpene ozonolysis experiment, utilizing a
 598 nitrate-based CI-APi-TOF (resolving power of 13000 Th/Th). Even a minor shift in the mass axis
 599 calibration could cause the signals of especially the yellow, green and blue peaks to change
 600 dramatically. Similarly, adding or removing an ion would alter the amount of signal attributed to the
 601 other fitted peaks.



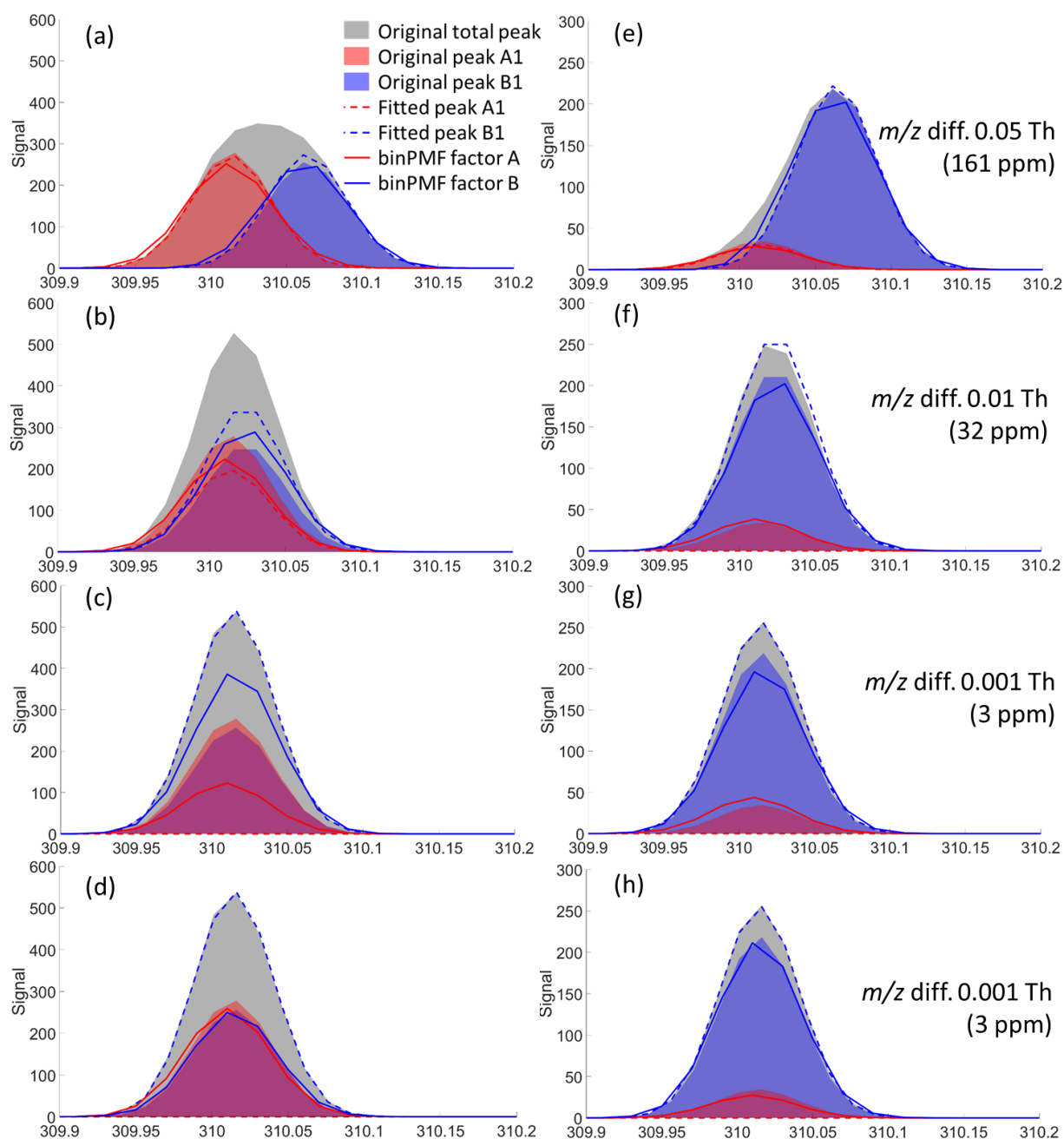
602

603 Figure 2. Conceptual comparison of traditional methods (UMR and HR) and binned mass spectra for
 604 PMF analysis. The raw data signal is shown in the left and contains eight ions. By UMR analysis, the
 605 information of the eight ions is totally lost. Using an analyst-determined peak-list, HR analysis
 606 attempts to separate signals at this mass by fitting selected ions. By binning the spectra, we utilize the
 607 HR information without any a priori information required.



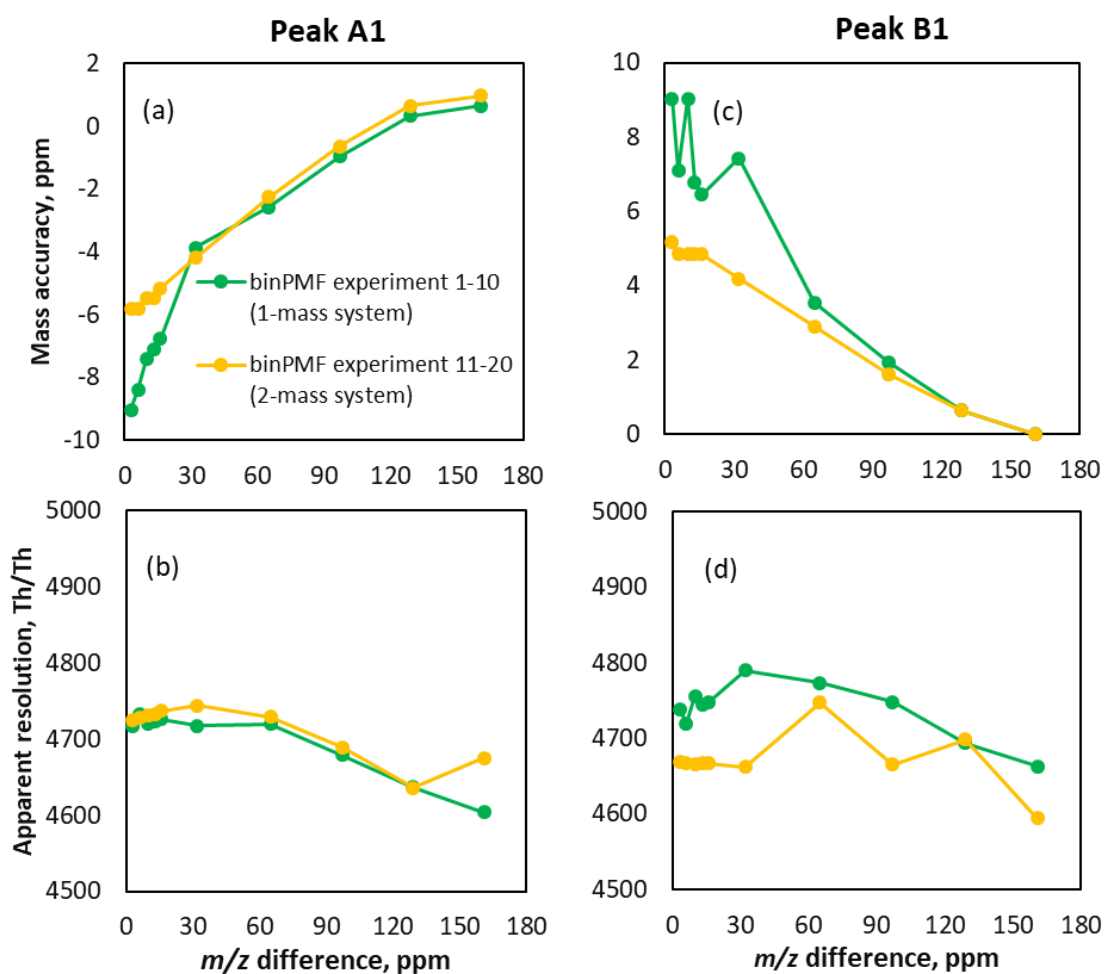
608

609 Figure 3. Conceptual schematic diagram for the synthetic datasets. Panels a and b describe
 610 experiments 1-10 in the one-mass system, panel c is experiments 11-20 in the two-mass system. Panel
 611 d shows experiment 21, with peaks A2 and B2 at separate integer masses (see text for details).



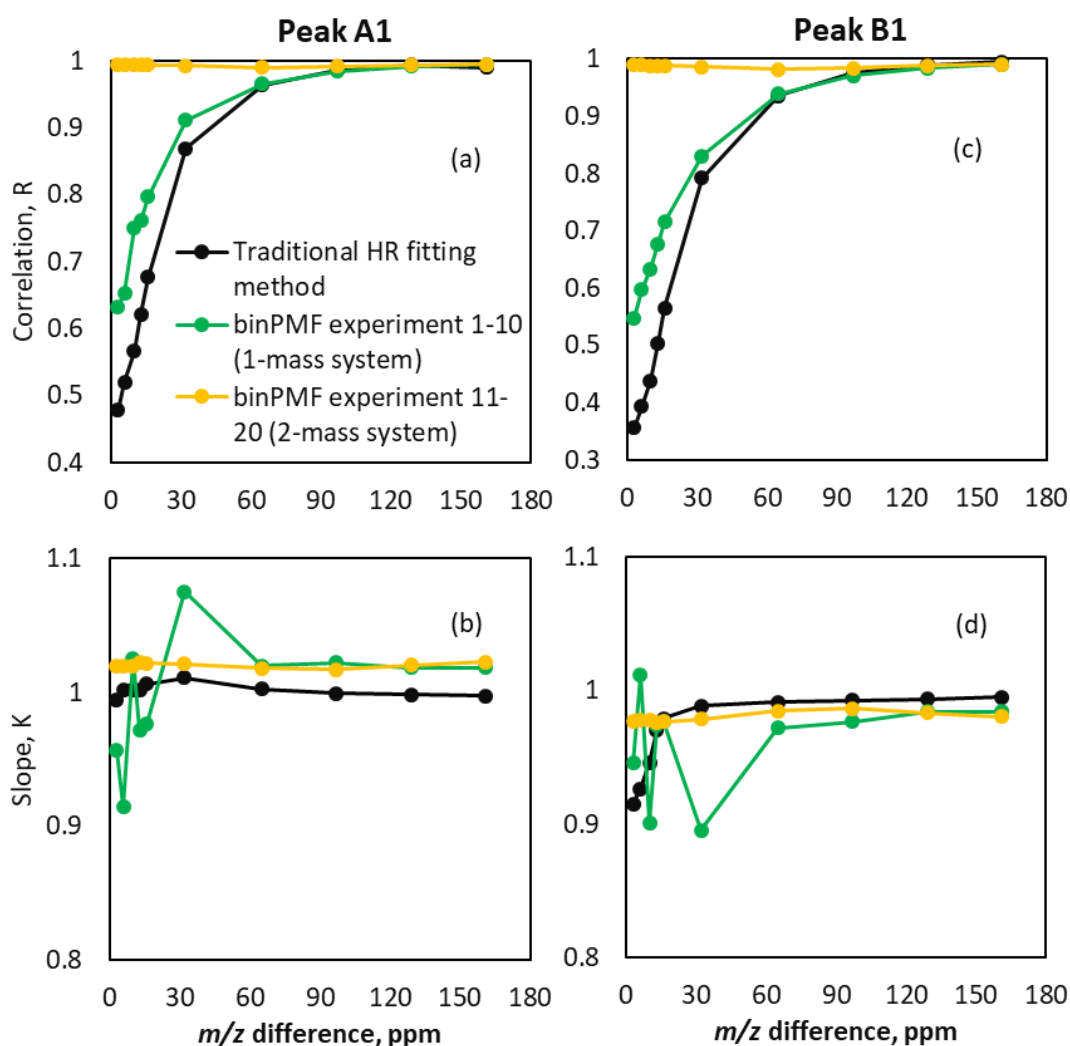
612

613 Figure 4. Peak separation results by a traditional HR fitting method (dashed lines) and binPMF (solid
 614 lines), at the 79th time point (panels a-d) and at the 21st time point (e-h) for experiment numbers 1 (a,
 615 e), 5 (b, f), 10 (c, g), and 20 (d, h). The signal intensity ratio of peaks A1 and B1 were about 1:1 and
 616 1:6, respectively, at the 79th and the 21st time points. Panels a-c and e-g are for the one-mass system,
 617 while panels d and h are for the two-mass system.



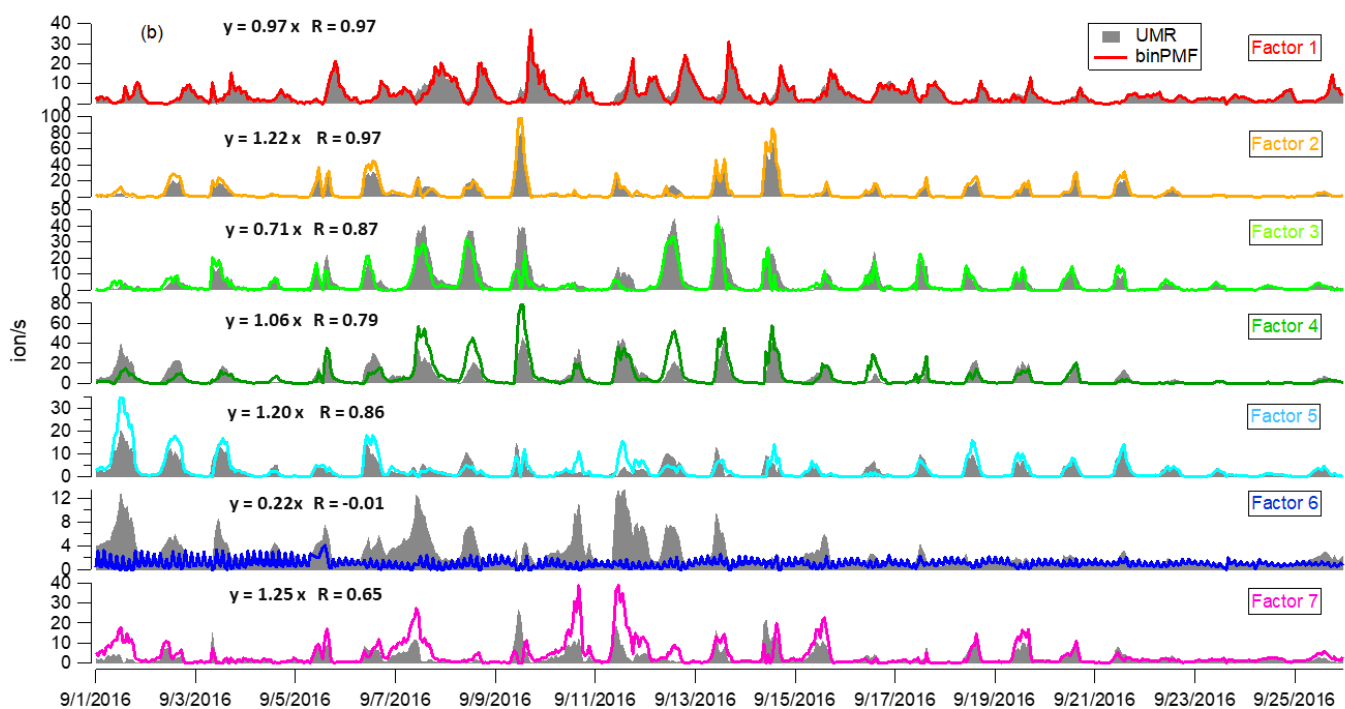
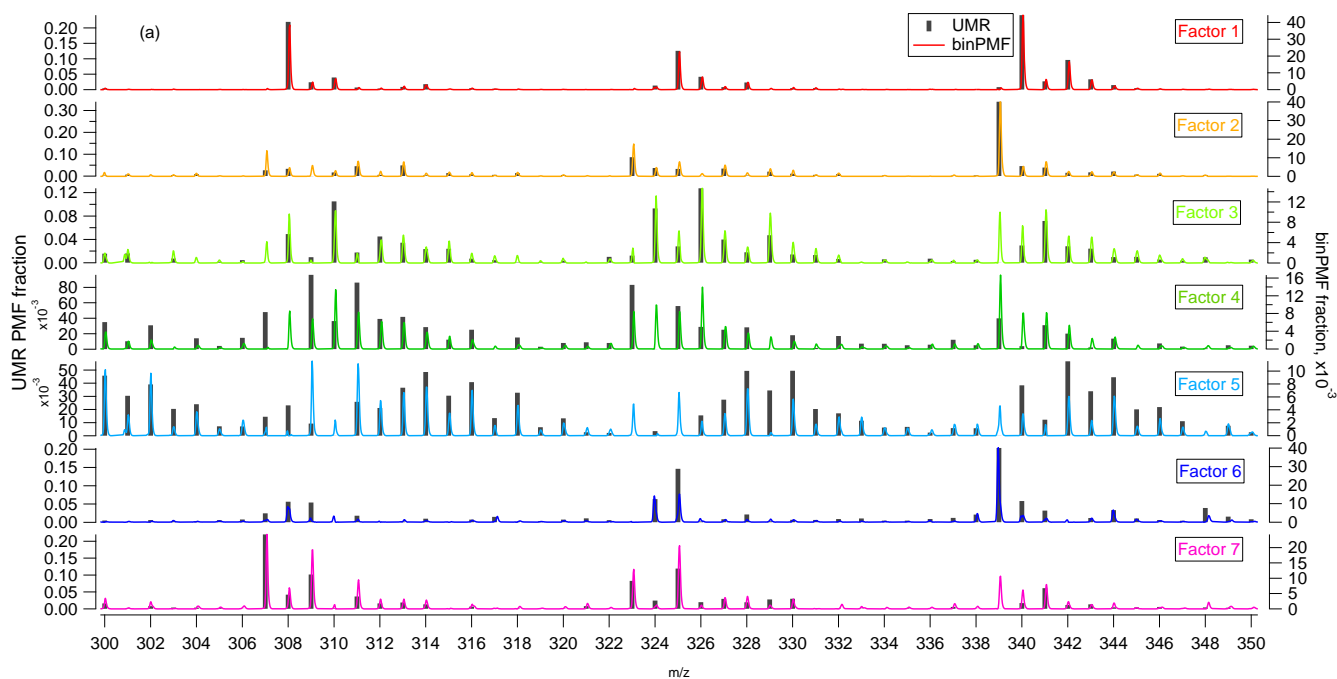
618

619 Figure 5. Characteristics of peaks fitted to binPMF factors. Panel a and b show results for peak A1,
 620 and c and d for peak B1. In panels a and c, the mass accuracy of peaks resolved by binPMF are
 621 compared to the original data. Panels b and d depict the resolution of the two fitted peaks. The original
 622 resolution of the input data was 5000 Th/Th.



623

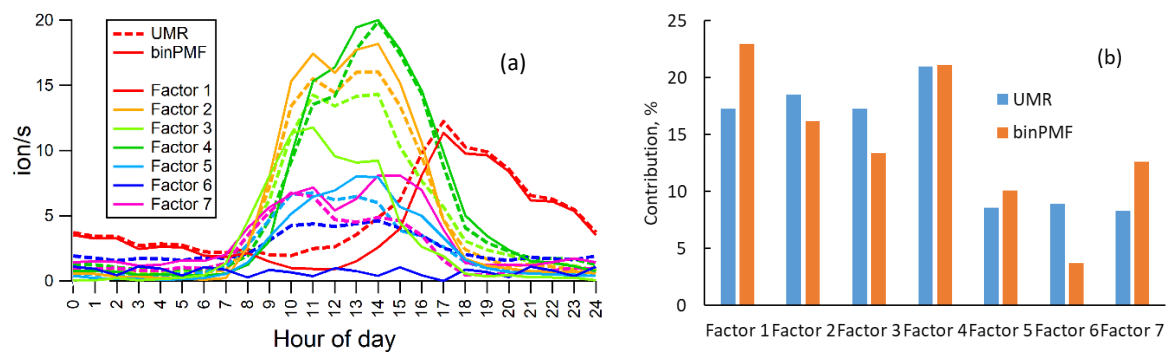
624 Figure 6. Comparison of time series of binPMF and HR fitting. Panel a and b show results for peak
 625 A1, and c and d for peak B1. Correlation of time series (panels a and c) retrieved by binPMF (green
 626 lines for experiments 1-10, yellow for 11-20) and traditional HR fitting (black lines) compared to
 627 original input data. Panels b and d depict the slope K of the linear fit $y = k \times x$, where y is the signal
 628 retrieved from the synthetic data by either binPMF or the HR fitting, and x is the original input signals.



629

630

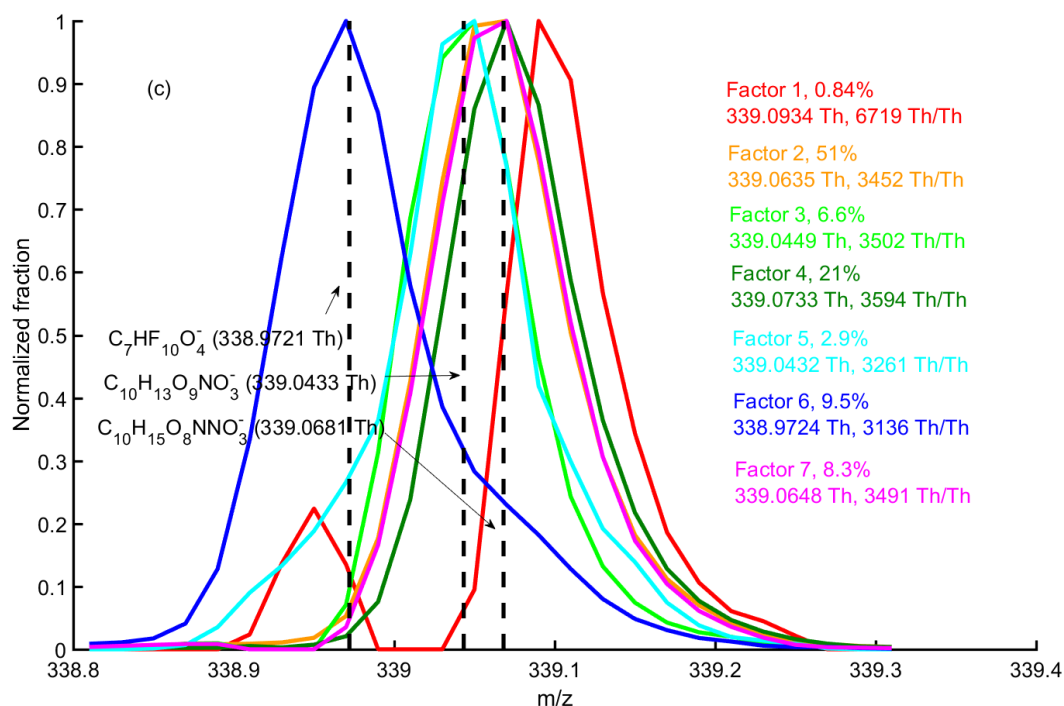
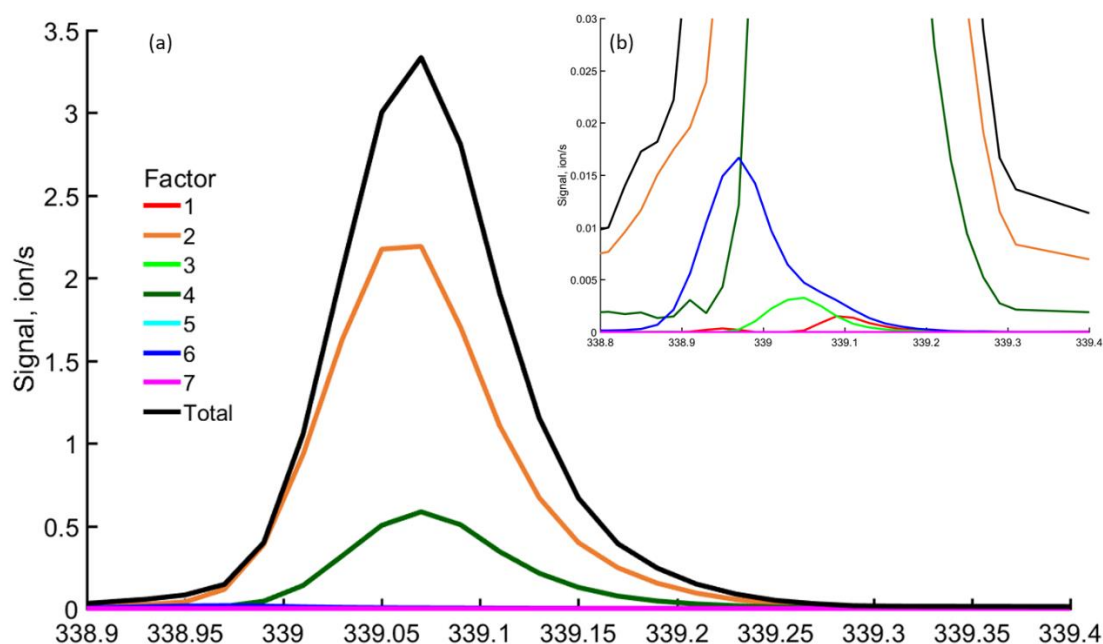
631 Figure 7. Comparison of binPMF and UMR-PMF for factor mass spectral profiles (panel a) and time
 632 series (panel b). The equations in each panel describe how signals from binPMF (y) compare with
 633 the UMR-PMF solution (x). R is the correlation coefficient between the time series.



634

635

Figure 8. Comparison of binPMF and UMR-PMF for (a) diurnal trend and (b) factor contribution



637

638 Figure 9. binPMF factor profiles at m/z 339 Th at 12:00 on September 9th. Panels a and b show the
 639 absolute concentrations of each factor, while in panel c, the factor profiles are normalized to the same
 640 maximum peak heights. The fitted peak location (Th) and the apparent resolution (Th/Th) for each
 641 factor is given in panel c,. The contribution of different factors to the integer m/z 339 Th is shown as
 642 a percentage. Three potential chemical compositions were marked with black vertical dashed lines.

643 **References**

- 644 Allan, J. D., Jimenez, J. L., Williams, P. I., Alfarra, M. R., Bower, K. N., Jayne, J. T., Coe, H., and Worsnop,
645 D. R.: Quantitative sampling using an Aerodyne aerosol mass spectrometer I. Techniques of data
646 interpretation and error analysis, *Journal of Geophysical Research: Atmospheres*, 108, 2003.
- 647 Bertram, T. H., Kimmel, J. R., Crisp, T. A., Ryder, O. S., Yatavelli, R. L. N., Thornton, J. A., Cubison, M. J.,
648 Gonin, M., and Worsnop, D. R.: A field-deployable, chemical ionization time-of-flight mass spectrometer,
649 *Atmos. Meas. Tech.*, 4, 1471-1479, 10.5194/amt-4-1471-2011, 2011.
- 650 Brown, S. G., Eberly, S., Paatero, P., and Norris, G. A.: Methods for estimating uncertainty in PMF
651 solutions: Examples with ambient air and water quality data and guidance on reporting PMF results, *Science*
652 *of The Total Environment*, 518-519, 626-635, <https://doi.org/10.1016/j.scitotenv.2015.01.022>, 2015.
- 653 Canagaratna, M., Jayne, J., Jimenez, J., Allan, J., Alfarra, M., Zhang, Q., Onasch, T., Drewnick, F., Coe, H.,
654 and Middlebrook, A.: Chemical and microphysical characterization of ambient aerosols with the aerodyne
655 aerosol mass spectrometer, *Mass Spectrometry Reviews*, 26, 185-222, 2007.
- 656 Canonaco, F., Crippa, M., Slowik, J., Baltensperger, U., and Prévôt, A.: SoFi, an IGOR-based interface for
657 the efficient use of the generalized multilinear engine (ME-2) for the source apportionment: ME-2
658 application to aerosol mass spectrometer data, *Atmospheric Measurement Techniques*, 6, 3649, 2013.
- 659 Corbin, J. C., Othman, A., Allan, J. D., Worsnop, D. R., Haskins, J. D., Sierau, B., Lohmann, U., and
660 Mensah, A. A.: Peak-fitting and integration imprecision in the Aerodyne aerosol mass spectrometer: effects
661 of mass accuracy on location-constrained fits, *Atmos. Meas. Tech.*, 8, 4615-4636, 10.5194/amt-8-4615-2015,
662 2015.
- 663 Craven, J. S., Yee, L. D., Ng, N. L., Canagaratna, M. R., Loza, C. L., Schilling, K. A., Yatavelli, R. L. N.,
664 Thornton, J. A., Ziemann, P. J., Flagan, R. C., and Seinfeld, J. H.: Analysis of secondary organic aerosol
665 formation and aging using positive matrix factorization of high-resolution aerosol mass spectra: application
666 to the dodecane low-NO_x system, *Atmos. Chem. Phys.*, 12, 11795-11817, 10.5194/acp-12-
667 11795-2012, 2012.
- 668 Cubison, M. J., and Jimenez, J. L.: Statistical precision of the intensities retrieved from constrained fitting of
669 overlapping peaks in high-resolution mass spectra, *Atmos. Meas. Tech.*, 8, 2333-2345, 10.5194/amt-8-2333-
670 2015, 2015.
- 671 Ehn, M., Kleist, E., Junninen, H., Petäjä, T., Lönn, G., Schobesberger, S., Dal Maso, M., Trimborn, A.,
672 Kulmala, M., Worsnop, D. R., Wahner, A., Wildt, J., and Mentel, T. F.: Gas phase formation of extremely
673 oxidized pinene reaction products in chamber and ambient air, *Atmos. Chem. Phys.*, 12, 5113-5127,
674 10.5194/acp-12-5113-2012, 2012.
- 675 Ehn, M., Thornton, J. A., Kleist, E., Sipila, M., Junninen, H., Pullinen, I., Springer, M., Rubach, F.,
676 Tillmann, R., Lee, B., Lopez-Hilfiker, F., Andres, S., Acir, I.-H., Rissanen, M., Jokinen, T., Schobesberger,
677 S., Kangasluoma, J., Kontkanen, J., Nieminen, T., Kurten, T., Nielsen, L. B., Jorgensen, S., Kjaergaard, H.
678 G., Canagaratna, M., Dal Maso, M., Berndt, T., Petaja, T., Wahner, A., Kerminen, V.-M., Kulmala, M.,
679 Worsnop, D. R., Wildt, J., and Mentel, T. F.: A large source of low-volatility secondary organic aerosol,
680 *Nature*, 506, 476-+, 10.1038/nature13032, 2014.
- 681 Guenther, A., Hewitt, C. N., Erickson, D., Fall, R., Geron, C., Graedel, T., Harley, P., Klinger, L., Lerdau,
682 M., McKay, W. A., Pierce, T., Scholes, B., Steinbrecher, R., Tallamraju, R., Taylor, J., and Zimmerman, P.:
683 A GLOBAL-MODEL OF NATURAL VOLATILE ORGANIC-COMPOUND EMISSIONS, *Journal of*
684 *Geophysical Research-Atmospheres*, 100, 8873-8892, 10.1029/94jd02950, 1995.
- 685 Hakola, H., Tarvainen, V., Bäck, J., Ranta, H., Bonn, B., Rinne, J., and Kulmala, M.: Seasonal variation of
686 mono- and sesquiterpene emission rates of Scots pine, *Biogeosciences*, 3, 93-101, 10.5194/bg-3-93-2006,
687 2006.
- 688 Hari, P., and Kulmala, M.: Station for Measuring Ecosystem–Atmosphere Relations (SMEAR II), *Boreal*
689 *Environment Research*, 10, 315-322, 2005.
- 690 Heinritzi, M., Simon, M., Steiner, G., Wagner, A. C., Kürten, A., Hansel, A., and Curtius, J.:
691 Characterization of the mass-dependent transmission efficiency of a CIMS, *Atmos. Meas. Tech.*, 9, 1449-
692 1460, 10.5194/amt-9-1449-2016, 2016.
- 693 Henry, R. C.: Current factor analysis receptor models are ill-posed, *Atmospheric Environment* (1967), 21,
694 1815-1820, [https://doi.org/10.1016/0004-6981\(87\)90122-3](https://doi.org/10.1016/0004-6981(87)90122-3), 1987.

695 Huang, S., Rahn, K. A., and Arimoto, R.: Testing and optimizing two factor-analysis techniques on aerosol
696 at Narragansett, Rhode Island, *Atmospheric Environment*, 33, 2169-2185, [https://doi.org/10.1016/S1352-](https://doi.org/10.1016/S1352-2310(98)00324-0)
697 2310(98)00324-0, 1999.

698 Huey, L. G.: Measurement of trace atmospheric species by chemical ionization mass spectrometry:
699 Speciation of reactive nitrogen and future directions, *Mass Spectrometry Reviews*, 26, 166-184,
700 10.1002/mas.20118, 2007.

701 Jimenez, J. L., Canagaratna, M. R., Donahue, N. M., Prevot, A. S. H., Zhang, Q., Kroll, J. H., DeCarlo, P. F.,
702 Allan, J. D., Coe, H., Ng, N. L., Aiken, A. C., Docherty, K. S., Ulbrich, I. M., Grieshop, A. P., Robinson, A.
703 L., Duplissy, J., Smith, J. D., Wilson, K. R., Lanz, V. A., Hueglin, C., Sun, Y. L., Tian, J., Laaksonen, A.,
704 Raatikainen, T., Rautiainen, J., Vaattovaara, P., Ehn, M., Kulmala, M., Tomlinson, J. M., Collins, D. R.,
705 Cubison, M. J., Dunlea, J., Huffman, J. A., Onasch, T. B., Alfarra, M. R., Williams, P. I., Bower, K., Kondo,
706 Y., Schneider, J., Drewnick, F., Borrmann, S., Weimer, S., Demerjian, K., Salcedo, D., Cottrell, L., Griffin,
707 R., Takami, A., Miyoshi, T., Hatakeyama, S., Shimono, A., Sun, J. Y., Zhang, Y. M., Dzepina, K., Kimmel,
708 J. R., Sueper, D., Jayne, J. T., Herndon, S. C., Trimborn, A. M., Williams, L. R., Wood, E. C., Middlebrook,
709 A. M., Kolb, C. E., Baltensperger, U., and Worsnop, D. R.: Evolution of Organic Aerosols in the
710 Atmosphere, *Science*, 326, 1525-1529, 10.1126/science.1180353, 2009.

711 Jokinen, T., Sipilä, M., Junninen, H., Ehn, M., Lönn, G., Hakala, J., Petäjä, T., Mauldin Iii, R. L., Kulmala,
712 M., and Worsnop, D. R.: Atmospheric sulphuric acid and neutral cluster measurements using CI-API-TOF,
713 *Atmos. Chem. Phys.*, 12, 4117-4125, 10.5194/acp-12-4117-2012, 2012.

714 Jokinen, T., Berndt, T., Makkonen, R., Kerminen, V.-M., Junninen, H., Paasonen, P., Stratmann, F.,
715 Herrmann, H., Guenther, A. B., Worsnop, D. R., Kulmala, M., Ehn, M., and Sipila, M.: Production of
716 extremely low volatile organic compounds from biogenic emissions: Measured yields and atmospheric
717 implications, *Proceedings of the National Academy of Sciences of the United States of America*, 112, 7123-
718 7128, 10.1073/pnas.1423977112, 2015.

719 Junninen, H., Ehn, M., Petäjä, T., Luosujärvi, L., Kotiaho, T., Kostianinen, R., Rohner, U., Gonin, M., Fuhrer,
720 K., Kulmala, M., and Worsnop, D. R.: A high-resolution mass spectrometer to measure atmospheric ion
721 composition, *Atmos. Meas. Tech.*, 3, 1039-1053, 10.5194/amt-3-1039-2010, 2010.

722 Kirkby, J., Duplissy, J., Sengupta, K., Frege, C., Gordon, H., Williamson, C., Heinritzi, M., Simon, M., Yan,
723 C., Almeida, J., Troestl, J., Nieminen, T., Ortega, I. K., Wagner, R., Adamov, A., Amorim, A., Bernhammer,
724 A.-K., Bianchi, F., Breitenlechner, M., Brilke, S., Chen, X., Craven, J., Dias, A., Ehrhart, S., Flagan, R. C.,
725 Franchin, A., Fuchs, C., Guida, R., Hakala, J., Hoyle, C. R., Jokinen, T., Junninen, H., Kangasluoma, J.,
726 Kim, J., Krapf, M., Kuerten, A., Laaksonen, A., Lehtipalo, K., Makhmutov, V., Mathot, S., Molteni, U.,
727 Onnela, A., Peraekylae, O., Piel, F., Petaejae, T., Praplan, A. P., Pringle, K., Rap, A., Richards, N. A. D.,
728 Riipinen, I., Rissanen, M. P., Rondo, L., Sarnela, N., Schobesberger, S., Scott, C. E., Seinfeld, J. H., Sipilae,
729 M., Steiner, G., Stozhkov, Y., Stratmann, F., Tome, A., Virtanen, A., Vogel, A. L., Wagner, A. C., Wagner,
730 P. E., Weingartner, E., Wimmer, D., Winkler, P. M., Ye, P., Zhang, X., Hansel, A., Dommen, J., Donahue,
731 N. M., Worsnop, D. R., Baltensperger, U., Kulmala, M., Carslaw, K. S., and Curtius, J.: Ion-induced
732 nucleation of pure biogenic particles, *Nature*, 533, 521-+, 10.1038/nature17953, 2016.

733 Kroll, J. H., Donahue, N. M., Jimenez, J. L., Kessler, S. H., Canagaratna, M. R., Wilson, K. R., Altieri, K. E.,
734 Mazzoleni, L. R., Wozniak, A. S., and Bluhm, H.: Carbon oxidation state as a metric for describing the
735 chemistry of atmospheric organic aerosol, *Nature Chemistry*, 3, 133, 2011.

736 Lanz, V. A., Alfarra, M. R., Baltensperger, U., Buchmann, B., Hueglin, C., Szidat, S., Wehrli, M. N.,
737 Wacker, L., Weimer, S., Caseiro, A., Puxbaum, H., and Prevot, A. S. H.: Source Attribution of Submicron
738 Organic Aerosols during Wintertime Inversions by Advanced Factor Analysis of Aerosol Mass Spectra,
739 *Environmental Science & Technology*, 42, 214-220, 10.1021/es0707207, 2008.

740 Lee, B. H., Lopez-Hilfiker, F. D., Mohr, C., Kurtén, T., Worsnop, D. R., and Thornton, J. A.: An Iodide-
741 Adduct High-Resolution Time-of-Flight Chemical-Ionization Mass Spectrometer: Application to
742 Atmospheric Inorganic and Organic Compounds, *Environmental Science & Technology*, 48, 6309-6317,
743 10.1021/es500362a, 2014.

744 Massoli, P., Stark, H., Canagaratna, M. R., Krechmer, J. E., Xu, L., Ng, N. L., Mauldin, R. L., Yan, C.,
745 Kimmel, J., Misztal, P. K., Jimenez, J. L., Jayne, J. T., and Worsnop, D. R.: Ambient Measurements of
746 Highly Oxidized Gas-Phase Molecules during the Southern Oxidant and Aerosol Study (SOAS) 2013, *ACS*
747 *Earth and Space Chemistry*, 10.1021/acsearthspacechem.8b00028, 2018.

748 Paatero, P., and Tapper, U.: Positive matrix factorization: A non-negative factor model with optimal
749 utilization of error estimates of data values, *Environmetrics*, 5, 111-126, 1994.

Paatero, P.: Least squares formulation of robust non-negative factor analysis, *Chemometrics and Intelligent Laboratory Systems*, 37, 23-35, [https://doi.org/10.1016/S0169-7439\(96\)00044-5](https://doi.org/10.1016/S0169-7439(96)00044-5), 1997.

Paatero, P.: The Multilinear Engine—A Table-Driven, Least Squares Program for Solving Multilinear Problems, Including the n-Way Parallel Factor Analysis Model, *Journal of Computational and Graphical Statistics*, 8, 854-888, 10.1080/10618600.1999.10474853, 1999.

Paatero, P., Hopke, P. K., Song, X.-H., and Ramadan, Z.: Understanding and controlling rotations in factor analytic models, *Chemometrics and Intelligent Laboratory Systems*, 60, 253-264, [https://doi.org/10.1016/S0169-7439\(01\)00200-3](https://doi.org/10.1016/S0169-7439(01)00200-3), 2002.

Paatero, P., and Hopke, P. K.: Discarding or downweighting high-noise variables in factor analytic models, *Analytica Chimica Acta*, 490, 277-289, [https://doi.org/10.1016/S0003-2670\(02\)01643-4](https://doi.org/10.1016/S0003-2670(02)01643-4), 2003.

Paatero, P., Eberly, S., Brown, S. G., and Norris, G. A.: Methods for estimating uncertainty in factor analytic solutions, *Atmos. Meas. Tech.*, 7, 781-797, doi:10.5194/amt-7-781-2014, 2014.

Polissar, A. V., Hopke, P. K., Paatero, P., Malm, W. C., and Sisler, J. F.: Atmospheric aerosol over Alaska: 2. Elemental composition and sources, *Journal of Geophysical Research: Atmospheres*, 103, 19045-19057, 1998.

Pope III, C. A., Ezzati, M., and Dockery, D. W.: Fine-particulate air pollution and life expectancy in the United States, *New England Journal of Medicine*, 360, 376-386, 2009.

Schauer, J. J., Rogge, W. F., Hildemann, L. M., Mazurek, M. A., Cass, G. R., and Simoneit, B. R.: Source apportionment of airborne particulate matter using organic compounds as tracers, *Atmospheric Environment*, 30, 3837-3855, 1996.

Shiraiwa, M., Ueda, K., Pozzer, A., Lammel, G., Kampf, C. J., Fushimi, A., Enami, S., Arangio, A. M., Fröhlich-Nowoisky, J., Fujitani, Y., Furuyama, A., Lakey, P. S. J., Lelieveld, J., Lucas, K., Morino, Y., Pöschl, U., Takahama, S., Takami, A., Tong, H., Weber, B., Yoshino, A., and Sato, K.: Aerosol Health Effects from Molecular to Global Scales, *Environmental Science & Technology*, 51, 13545-13567, 10.1021/acs.est.7b04417, 2017.

Song, Y., Shao, M., Liu, Y., Lu, S., Kuster, W., Goldan, P., and Xie, S.: Source apportionment of ambient volatile organic compounds in Beijing, *Environmental science & technology*, 41, 4348-4353, 2007.

Stark, H., Yatavelli, R. L. N., Thompson, S. L., Kimmel, J. R., Cubison, M. J., Chhabra, P. S., Canagaratna, M. R., Jayne, J. T., Worsnop, D. R., and Jimenez, J. L.: Methods to extract molecular and bulk chemical information from series of complex mass spectra with limited mass resolution, *International Journal of Mass Spectrometry*, 389, 26-38, <https://doi.org/10.1016/j.ijms.2015.08.011>, 2015.

Stocker, T., Qin, D., Plattner, G., Tignor, M., Allen, S., Boschung, J., Nauels, A., Xia, Y., Bex, V., and Midgley, P.: IPCC, 2013: Climate Change 2013: The Physical Science Basis. Contribution of Working Group I to the Fifth Assessment Report of the Intergovernmental Panel on Climate Change, 1535 pp, in, Cambridge Univ. Press, Cambridge, UK, and New York, 2013.

Sun, Y.-L., Zhang, Q., Schwab, J., Demerjian, K., Chen, W.-N., Bae, M.-S., Hung, H.-M., Hogrefe, O., Frank, B., and Rattigan, O.: Characterization of the sources and processes of organic and inorganic aerosols in New York city with a high-resolution time-of-flight aerosol mass spectrometer, *Atmospheric Chemistry and Physics*, 11, 1581-1602, 2011.

Ulbrich, I. M., Canagaratna, M. R., Zhang, Q., Worsnop, D. R., and Jimenez, J. L.: Interpretation of organic components from Positive Matrix Factorization of aerosol mass spectrometric data, *Atmos. Chem. Phys.*, 9, 2891-2918, 10.5194/acp-9-2891-2009, 2009.

Wei, W., Wang, S., Chatani, S., Klimont, Z., Cofala, J., and Hao, J.: Emission and speciation of non-methane volatile organic compounds from anthropogenic sources in China, *Atmospheric Environment*, 42, 4976-4988, <https://doi.org/10.1016/j.atmosenv.2008.02.044>, 2008.

Yan, C., Nie, W., Aijala, M., Rissanen, M. P., Canagaratna, M. R., Massoli, P., Junninen, H., Jokinen, T., Sarnela, N., Hame, S. A. K., Schobesberger, S., Canonaco, F., Yao, L., Prevot, A. S. H., Petaja, T., Kulmala, M., Sipila, M., Worsnop, D. R., and Ehn, M.: Source characterization of highly oxidized multifunctional compounds in a boreal forest environment using positive matrix factorization, *Atmospheric Chemistry and Physics*, 16, 12715-12731, 10.5194/acp-16-12715-2016, 2016.

Zha, Q., Yan, C., Junninen, H., Riva, M., Sarnela, N., Aalto, J., Quéléver, L., Schallhart, S., Dada, L., Heikkinen, L., Peräkylä, O., Zou, J., Rose, C., Wang, Y., Mammarella, I., Katul, G., Vesala, T., Worsnop, D. R., Kulmala, M., Petäjä, T., Bianchi, F., and Ehn, M.: Vertical characterization of highly oxygenated molecules (HOMs) below and above a boreal forest canopy, *Atmos. Chem. Phys.*, 18, 17437-17450, 10.5194/acp-18-17437-2018, 2018.

805 Zhang, Q., Jimenez, J. L., Canagaratna, M., Allan, J., Coe, H., Ulbrich, I., Alfarra, M., Takami, A.,
 806 Middlebrook, A., and Sun, Y.: Ubiquity and dominance of oxygenated species in organic aerosols in
 807 anthropogenically-influenced Northern Hemisphere midlatitudes, *Geophysical Research Letters*, 34, 2007.
 808 Zhang, Q., Jimenez, J. L., Canagaratna, M. R., Ulbrich, I. M., Ng, N. L., Worsnop, D. R., and Sun, Y.:
 809 Understanding atmospheric organic aerosols via factor analysis of aerosol mass spectrometry: a review,
 810 *Analytical and Bioanalytical Chemistry*, 401, 3045-3067, 10.1007/s00216-011-5355-y, 2011.
 811 Zhang, Y., Lin, Y., Cai, J., Liu, Y., Hong, L., Qin, M., Zhao, Y., Ma, J., Wang, X., and Zhu, T.: Atmospheric
 812 PAHs in North China: spatial distribution and sources, *Science of the Total Environment*, 565, 994-1000,
 813 2016.
 814 Zhang, Y., Cai, J., Wang, S., He, K., and Zheng, M.: Review of receptor-based source apportionment
 815 research of fine particulate matter and its challenges in China, *Science of the Total Environment*, 586, 917-
 816 929, 2017.

817

818